

Implementing robust thermodynamic model for reliable bubble/dew problem solution in cryogenic distillation of air separation units

Filippo Bisotti^a, Andrea Galeazzi^a, Luca Galatioto^b, Fabio Masserdotti^b, Alessandro Bigi^b, Pierluigi Gritti^b, Flavio Manenti^{a,*}

^a Politecnico di Milano, CMIC Dept. "Giulio Natta", Piazza Leonardo da Vinci 32, 20133 Milan, Italy

^b SIAD Macchine e Impianti, Via San Bernardino 92, 24100 Bergamo, Italy

ARTICLE INFO

Article History:

Received 21 December 2020

Revised 1 March 2021

Accepted 16 March 2021

Available online 26 March 2021

Keywords:

Air mixture

Air separation units

Bender equation of state

Bubble and dew point problems

Non-cubic equation of state (NCEoS)

Robust and efficient algorithm

ABSTRACT

High accuracy in Equations of State (EoSs) is becoming a more and more critical aspect for design and operational purposes in different areas of chemical and process engineering. It is well-known that improper predictions of mixture properties provide large deviations in process simulations, process control actions, estimation of operative conditions, assessment of performance indexes and optimal unit/process design. These deviations are strongly emphasized when typical operating conditions appear rather severe. One of the most challenging application sectors is represented by cryogenic separations and especially in case their nominal operating conditions approach the critical point. Air Separation Units (ASUs) are the ideal application field to demonstrate these criticisms. In addition, dedicated EoS sometimes lacks in implementation details and thermodynamic parameters, making the reliability target impossible to be achieved. The present paper is aimed at bridging the current gaps in the implementation of Bender EoS for the reliable prediction of air mixture properties as well as the reliable simulation of ASU plants. The implementation requires the description of robust and efficient algorithms. At last, a quantitative comparison between the proposed approach and the existing solutions is provided.

© 2021 The Author(s). Published by Elsevier Ltd. This is an open access article under the CC BY license (<http://creativecommons.org/licenses/by/4.0/>)

1. Introduction

Accurate thermodynamic modeling is fundamental for a precise prediction of fluid properties, especially in the case of mixtures. The demand for high accuracy thermodynamic models has always been very high and it is also ever-increasing due to the necessity of processes optimization and energy efficiency [13,31,38,39,46,66]. Process System Engineering could be represented as a series of interconnected layers and in this image, the thermodynamic modelling and consequent robust-efficient properties estimation algorithms are the core of this structure [27]. It is well-known that more accurate predictions result in a more reliable process design parameters estimation [11,17,20,23,53,55,67], an optimal operative conditions definition [16,18,35,77,95,97], a better units design, a more clear estimation of investment and operative costs [39], more performing process control and a higher reduction in energy consumption [56,60,71].

In the 1970s, the request for accurate thermodynamic models was partially satisfied by Cubic Equations of State (CEoS) such as, for example, the Soave-Redlich-Kwong (SRK) CEOs [76], and the Peng-Robinson (PR) CEOs [62]. Their developments were originally based

on physical principles and they had a theoretical background. They are still considered as best practice in many areas of application given their easiness in numerical implementation (i.e., availability of the analytical solution) and domain application adaptability [3,9,19,61].

CEOEs offer the opportunity to develop modified relationships based on their original structures, for instance, PR EoS are modified, mainly:

- In the energy terms [52,85] with theoretical studies on the definition of the main parameters involved [43];
- In the estimation of the coefficients for enlarging the feasible domain towards the critical point [14,36,65];
- On the mixing rule parameters [85,91];
- By introducing additional terms to increase prediction accuracy and flexibility [85].

Remarkably modified PR-type EoS have an increased number of parameters and they are called three- and four-parameters EoS. Some examples are reported as:

- PTV, reported by Patel-Teja-Valderrama [25,59,86];
- PRSV, developed by Stryjek-Vera [78,79];
- TB, proposed by Trebble-Bishnoi [82–84].

* Corresponding author.

E-mail address: flavio.manenti@polimi.it (F. Manenti).



List of symbols

P	Pressure [kPa]
T	Temperature [K]
d_m	Molar density [mol/L]
R	Ideal gas constant [J/(mol·K)]
z_k	k compound generic phase molar fraction
x_k	k compound liquid molar fraction
y_k	k compound vapour molar fraction
\mathbf{z}	Composition vector
\mathbf{x}	Liquid phase composition vector
\mathbf{y}	Vapour phase composition vector
$a_{i,k}$	i-th Bender fitting parameters for k pure component (see Appendix A)
a_i, B, C, D, E, F, G, H	Mixing coefficient in Eq. (1) (see Appendix A)
a_i^F, B_F, C_F etc	Mixing coefficient in fugacity definition Eq. (3) (see Appendix A)
<i>Subscripts and superscripts</i>	
k	Index for component: Nitrogen (1), Argon (2) and Oxygen (3)
i	Index for Bender fitting coefficients for pure components ($i = 1, 2, 3, \dots, 20$)
N_2	Nitrogen
Ar	Argon
O_2	Oxygen
vap	Vapour phase
liq	Liquid phase
F	Fugacity coefficients subscript
V	Vapour phase superscripts
L	Liquid phase superscript
<i>Greek letters</i>	
$\hat{\phi}$	Fugacity coefficient in mixture
Ω	Omega function Eq. (7)
Θ	Exponent of fugacity coefficient Eq. (3)
α, β, γ	Matrix elements (see Appendix A)
ε	Relative error
<i>Acronyms</i>	
ASU	Air Separation Unit(s)
BWR	Benedict Weber Rubin NCEoS
EoS	Equation of State
CEoS	Cubic-type Equation of State
NCEoS	Non-Cubic Equation of State
NLS	Non-Linear System
PR	Peng-Robinson (EoS)
SRK	Soave-Redlich-Kwong (EoS)

that all the impurities, including carbon dioxide, are preventively removed, the purified air mixture is an ideal field for NCEoS development, validation, and application. For this reason, one of the most widespread thermodynamic model adopted in Air Separation Units (ASU) simulation and optimization, both in scientific and technical or industrial communities, is the Bender NCEoS [5,7,26,72,94].

ASUs have been thoroughly analysed from different points of view: optimal process design, static and dynamic simulation [2,54,92,97], thermodynamic modelling [37,48,73,88], integration and coupling with other plants [35,50], and finally optimization and operation planning [34,95,96]. Many engineering, procurement, and construction (EPC) companies working in the ASU business emphasised some issues and troubles related to ASU design and operation especially in terms of the reliability in thermodynamic models of the side-column for argon-oxygen splitting and thermal efficiency of the cold box [2,54,87,92]. Thermodynamic models are the primary aspect for overcoming these difficulties and improvements have been made in this direction. In fact, all the experimental campaigns performed since the 1950s indicate that there is a high interest in obtaining accurate data needed to improve thermodynamic model prediction reliability, as reported in several works [22,42,48]. Lemmon et al. also report some of the most relevant works concerning experimental data campaigns on air mixtures. More recently, some works have tried to compare the performance of different EoS suitable for ASU simulation. As reported in Fu and Selinger works [26,72], a modified version of PR CEoS and Bender models are the most used thermodynamic models to simulate and design ASU despite the focus of the past years to improve BWR NCEoS [37,73,88]. However, Bender NCEoS is currently the most reliable and established thermodynamic model for industrial applications [33,94] although it is not directly implemented in the most common process simulators (e.g. AspenOne Suite, PRO II, and UniSim Design). The Bender NCEoS success could be explained by the failure of the modified PR equations of state since they show several numerical issues with a decrease in reliability in some portions of the operative condition domain, especially close to the triple point and in some cases also close to the critical one [33]. Nevertheless, a proper handling of Bender NCEoS is required in order to obtain reliable and accurate results due to its intrinsic nonlinearity.

Thanks to its tuneable accuracy, Bender's model has been also applied to other mixtures, such as ethylene and propylene [4,10], but also to more complex mixtures such as natural gas, for instance, methane, propane, n-butane, and n-pentane [15,29,74,80]. Some attempts to generalize the Bender model for accounting more components and in wider applicability ranges are present in literature [68–70]. Also, some applications in the field of carbon capture and sequestration have also been implemented [32].

Despite all the above improvements and attempts to provide accurate thermodynamic models, the main issue is still the robustness of the numerical solution. Many researchers implemented efficient algorithms for CEoS in process simulators in order to reduce the computational effort, also increasing numerical accuracy while others proposed several numerical techniques to effectively calculate mixtures thermodynamic properties such as compressibility factor and so forth also close to the critical point [30,44,45].

This is not yet the case for the Bender NCEoS and, more in general, the NCEoS family.

In this paper, the Bender NCEoS is introduced in Section 2. A robust and efficient algorithm to solve both bubble and dew problems is proposed in Section 3. The case study and related results are provided in Section 4. In particular, the implemented algorithm and NCEoS are compared to the NIST NCEoS [48] for the dry air mixture. The NIST NCEoS has been set as a reference due to its high accuracy (relative error generally less than 0.5%). This work aims at proposing a suitable algorithm to solve the bubble and dew problem. The proposed procedure may be applied for other NCEoS.

To achieve additional reliability in predictions, recently many research activities have been focused on the development of Non-Cubic EoS (NCEoS) for both pure compounds and mixtures, which are not any longer based on theoretical principles, but derive from dedicated experimental data fitting [41,48].

Nevertheless, their application field is still rather limited to few components since the computational effort required is rather costly [21,47,49,51,90,93].

An extensive application area for the NCEoS is represented by air liquefaction which involves, actually, few components: nitrogen, oxygen, argon, carbon dioxide, and several other impurities, mainly traces of nitrous oxides and light hydrocarbons [1,24,81]. Assuming

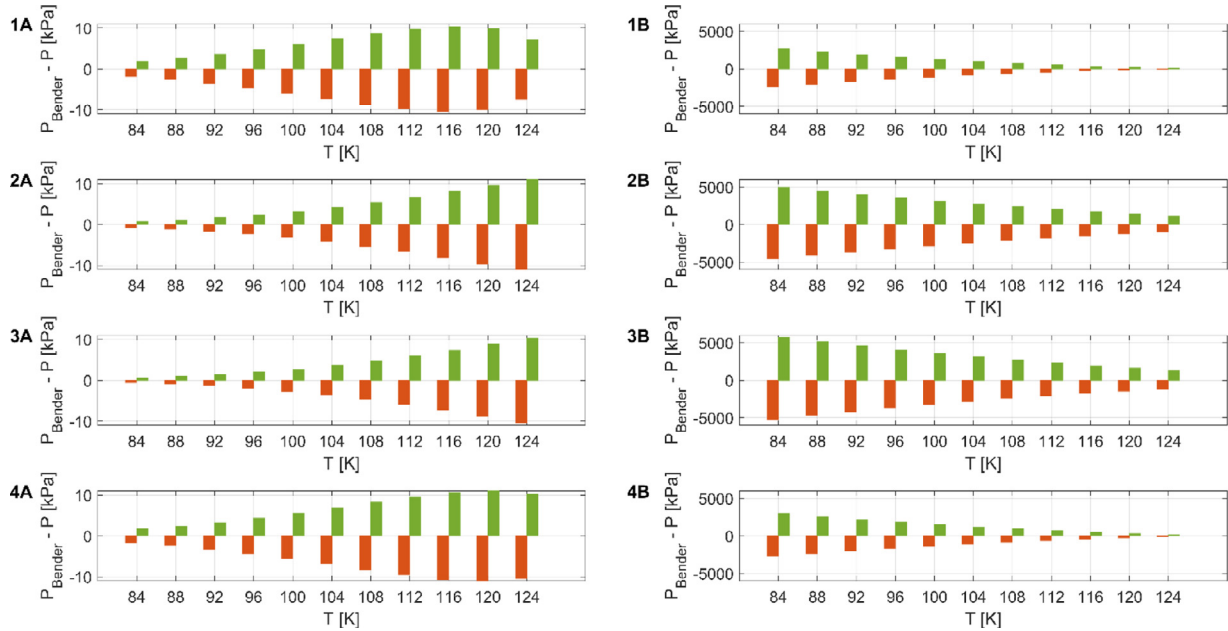


Fig. 1. Error in pressure prediction for deviation (+1% green and -1% red bar) around the phase density root (A – vapour and B – liquid phase) for different ternary mixtures with different oxygen contents: (1) N₂-rich, (2) Ar-rich, (3) O₂-rich, and (4) dry air. Data are reported from Bender's work appendix.

2. Bender equation of state: general function shapes and features

Bender NCEoS is a development of the Benedict-Rubin-Weber (BWR) NCEoS specifically tailored for the air components, i.e., nitrogen, argon, and oxygen. Bender provided a set of twenty fitted coefficients for each pure component and suitable mixing rules (i.e., linear, geometric, and Lorentz-type) to evaluate the corresponding mixing parameters. Those coefficients directly derive from regressions performed on experimental data and they are available on Bender's works [5–7]. Techniques and strategies for numerical regression are reported in the same works. As stated by Bender, among the many empirical equations of state published, only two have been largely applied for predicting phase equilibria in the nitrogen-argon-oxygen system. It is well known that BWR NCEoS is not suitable for use in the liquid region of both pure fluid and mixtures. Whereas SRK and PR CEoS, despite their capacity to easily fit experimental pressure-temperature-volume data at low-density gas region or those of the liquid region, have unique sets of coefficients that, even if these are temperature dependent, are not able to provide good accuracy and reliability on the whole range of temperature and pressure. Bender NCEoS tries to achieve a good representation of the gas region as well as of the condensed phase including the two-phase region with one single function (E. Bender, 1973). The constitutive relationship among pressure, temperature, composition, and molar density (d_m) is given

$$P_{\text{EOS}}(T, d_m, z) = d_m T \left[R + \left(a_1 - \frac{a_2}{T} - B \right) d_m + C d_m^2 + D d_m^3 + E d_m^4 + F d_m^5 + (G + H d_m^2) d_m^2 \cdot \exp(-a_{20} d_m^2) \right] \quad (1)$$

Mixing coefficients and corresponding rules are also available in the literature and a smart implementation exploiting matrix and vector products to speed up calculations has been already proposed [8]. This procedure is especially recommended in phase equilibria problems in order to avoid repetitive time-consuming operations. Bender provided also the expression for the fugacity in a mixture of each component. As in the previous case, the mixture coefficients are analytically evaluable and matrix-vector products are suggested. For more details see appendix A.

$$\hat{\phi}_k(T, d_m, z) = RT d_m z_k \cdot \exp(\theta) \quad (2)$$

where the exponent is defined as follows

$$\theta(T, d_m, z) = \frac{1}{R} \cdot \left\{ \left(a_1^F + \frac{2a_2^F}{T} - 2B_F \right) d_m + \frac{3}{2} C_F d_m^2 + D_F d_m^3 + E_F d_m^4 + F_F d_m^5 \right. \\ \left. + \left[\beta_1 - \beta_2 - (\beta_3 + \beta_4) \left(\frac{a_{20,k}}{a_{20}} \right)^{\frac{1}{2}} \right] d_m^2 \right\} \quad (3)$$

The main issue concerning the Bender NCEoS is the steepness of the constitutive law around the density root: when a small density variation occurs the pressure value error is greatly magnified. Indeed, as shown in Fig. 1, for a displacement of 1% around the correct molar density value the pressure predictions, according to Eq. (1), are highly affected. This demonstrates that the Bender model is strongly steep around the density root, especially for the liquid phase which is very common for CEoS and NCEoS. Function steepness decreases for temperature increment and it is inversely proportional to the oxygen and argon content. These trends are fully understandable in the light of the numerical techniques that Bender applied to obtain the fitting parameters for pure compounds [5].

The sensitivity analysis has been conducted on both ternary and binary mixtures. The results are reported in Figs. 1 and 2 for ternary mixtures whereas for binary mixtures in Appendix C. The sensitivity analysis has been mainly devoted to identifying the steepness of Bender function around the density solution. In Fig. 1 it is shown the pressure variation for increment (green bar) and decrement (red bar) of 1% of density phase. Fig. 2 depicts the derivatives in the density root point. Four ternary mixtures have been analysed: composition vectors are here ordered as $\mathbf{z} = [\text{N}_2 \text{ Ar} \text{ O}_2]$:

- N₂ - rich mixture $\mathbf{z} = [0.95 \ 0.005 \ 0.045]$
- Ar - rich mixture $\mathbf{z} = [0.05 \ 0.855 \ 0.095]$
- O₂ - rich mixture $\mathbf{z} = [0.05 \ 0.095 \ 0.855]$
- Dry air $\mathbf{z} = [0.80 \ 0.02 \ 0.18]$

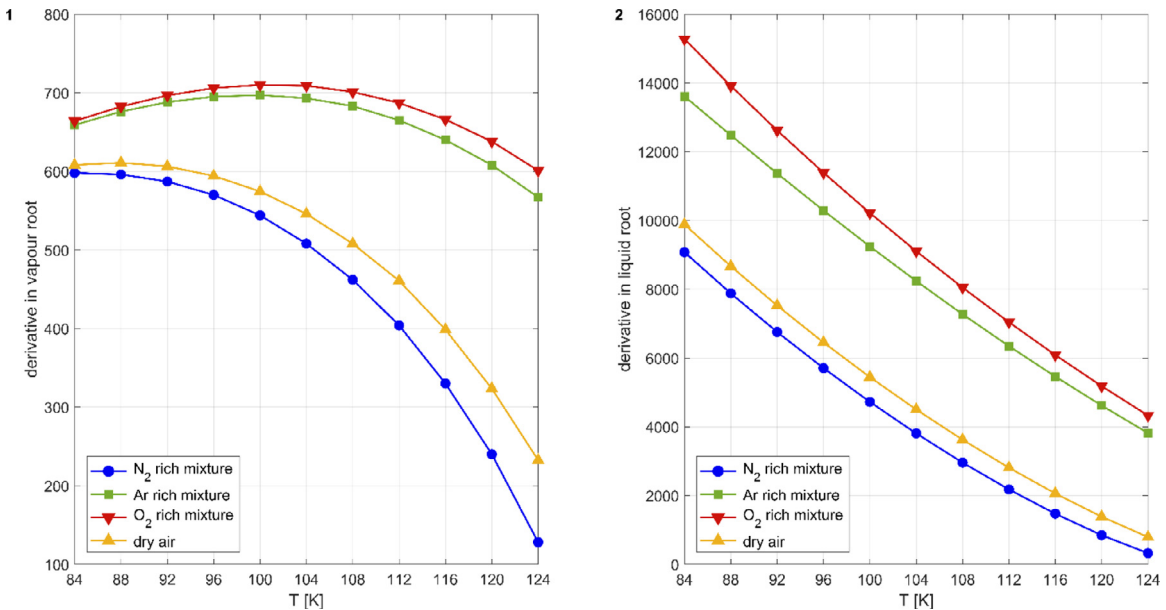


Fig. 2. Derivations in the phase density root point (1 – vapour and 2 – liquid) for different mixtures composition: N₂-rich (blue), Ar-rich (green), O₂-rich (red) mixtures, and dry air (yellow). Compositions are ordered as listed in Fig. 1. (For interpretation of the references to colour in this figure legend, the reader is referred to the web version of this article.)

Moreover, the derivative in density-root point has been evaluated and the results are reported in Fig. 2. This chart shows once again that Bender NCEoS is a steep function in the root point. This means that the gradient-oriented Non-Linear System (NLS) solver should be opportunely tuned in order to guarantee convergence.

To summarize, these Fig.s depict the general features of the Bender NCEoS:

- The steepness around phase density solution especially for vapour phase;
- The steepness is directly related to the mixture composition: mixtures enriched in nitrogen exhibit a more regular profile, while the worst case is represented by mixtures containing mainly oxygen;
- The deviations in vapour density are magnified for increasing temperatures, while the opposite is verified for liquid density;
- Larger errors associated with density deviation are encountered for high oxygen content both for vapour and liquid phase.

Further details for binary mixtures are reported in Appendix C.

2.1. Bubble and Dew problems formulation with Bender EoS

In bubble and dew problems when CEoS are applied, the unknowns are a thermodynamic variable (either temperature or pressure) and one phase composition, the vapor one for the bubble problem or the liquid one in the dew case [64,75]. Owing to the non-linear constitutive law interconnection among pressure, temperature, density, and composition, phase density is an additional unknown since the compressibility factor cannot be directly calculated. Therefore, the presence of molar densities as additional unknowns slightly modifies the system:

$$\left\{ \begin{array}{l} \hat{\phi}_k^V(T, d_V, y) \cdot y_k - \hat{\phi}_k^L(T, d_L, x) \cdot x_k = 0 \quad k = 1, 2, 3 \\ P_{EoS}^V(T, d_V, y) - P = 0 \\ P_{EoS}^L(T, d_L, x) - P = 0 \\ \sum_k x_k - 1 = 0 \text{ or } \sum_k y_k - 1 = 0 \end{array} \right. \quad (4)$$

$\hat{\phi}_k^{(\alpha)}$ is the fugacity coefficient in mixtures of the k component in the generic phase α coefficient and it is a function of temperature, phase density, and composition. In order to partially simplify the

system and guarantee phase composition consistency, it is worth removing the stoichiometry equation ensuring a molar fraction normalized composition (i.e., $y_3 = 1 - y_1 - y_2$ or $x_3 = 1 - x_1 - x_2$). Taking advantage of this substitution, the current system becomes:

$$\left\{ \begin{array}{l} \hat{\phi}_k^V(T, d_V, y_1, y_2) \cdot y_k - \hat{\phi}_k^L(T, d_L, x_1, x_2) \cdot x_k = 0 \quad k = 1, 2, 3 \\ P_{EoS}^V(T, d_V, y) - P = 0 \\ P_{EoS}^L(T, d_L, x) - P = 0 \end{array} \right. \quad (5)$$

3. Methods and algorithms

The development and the numerical strategies adopted to solve bubble and dew problems using Bender NCEoS will be described. Differently from what was presented in Bender's work, where simplified forms of bubble and dew problems have been partially dealt with, here, a solution strategy is proposed. Algorithms are proposed in a chronological evolution in order to emphasize additional issues that arise in each step and the numerical strategies adopted to improve the algorithm stability, reduce the computational time, and enhance the numerical precision. The algorithms have been implemented in Microsoft Visual Studio C++ 2013 and the numerical routines for the solution of the NLS have been taken from the BzzMath numerical library developed at Politecnico di Milano [12].

3.1. Standard algorithm and sensitivity analysis

The strategy adopted to achieve a numerical solution for NLS presented in Eq. (5) tries to decompose the global problem into simpler sub-problems. In this perspective, it is possible to handle smaller problems whose solution is less complex and time-consuming. The partial results of the different sub-problems enable to obtain of reliable values for the unknown variables. These partial results are then reused as guess values for the unknowns to solve the global problem in Eq. (5). More in detail, initially, it is worth removing the phase density dependence since it is an unknown of the problem and it appears both in Eq. (1) and Eqs. (2) and (3). Generally, in CEoS, the phase density can be calculated a posteriori once the compressibility factor has been estimated. In Bender's model, density is part of the thermodynamic model, hence, it is not possible to remove this dependence. The decoupling of pressure and fugacity is a key aspect to simplify

the general problem. Finally, considering that both nitrogen, argon, and oxygen are nonpolar compounds, it is acceptable that the liquid phase should not show a strong nonideal behaviour even in cryogenic conditions as already proven [28].

Taking advantage of that:

- Decoupling Eqs. (1) and (2) implies removing density dependence,
- N₂-Ar-O₂ liquid phase does not show deviation from ideal behaviour,

a simplified approach is to solve the Raoult law, as stated in Eq. (6). The Raoult problem solution provides as results temperature or pressure and the unknown phase composition independently from the density phase. Vapour tension relationships are taken from [63]

$$\begin{cases} P \cdot y_k - P_k^{\text{sat}}(T) \cdot x_k = 0 & k = 1, 2, 3 \\ \sum x_k - 1 = 0 \text{ or } \sum y_k - 1 = 0 \end{cases} \quad (6)$$

These partial results, now, are applied on the Bender EoS Eq. (1) to directly evaluate the corresponding phase density. Hence, the Raoult problem allows handling a simplified problem and, consequently, to build the first guess values to be provided to the original global nonlinear system Eq. (5). The standard algorithm works properly in the middle range, i.e., far from the triple and critical points. Indeed, close to these region boundaries, it is not able to reach a solution or the solution is even physically not acceptable. This instability is mainly related to general features of the Bender NCEoS previously explained and the possibility to violate feasible constraints imposed on thermodynamic variables. In Section 3.2 a proof on how to handle these infeasibilities is presented.

3.2. Robust algorithm implementation

To ensure stability on the whole domain, a sensitivity analysis has been done on the mixing parameters appearing in the constitutive relationship Eq. (1). This has been performed by changing composition at fixed temperatures. Temperature values have been selected to cover the whole vapor-liquid equilibrium region. The results of the sensitivity analysis are listed in Table 1. The 3D-charts and quantitative analysis are given in Appendix B. The 3D-charts provide a more detailed picture of the virial coefficient variation as a function of temperature and phase composition.

The sensitivity analysis shows that a few coefficients are not affected by the parameters variation while the majority is sensible at

Table 1
Dependence of main parameters temperature (T) and composition (z): (□) absence of dependence, (■) strong dependence, and (partially) means weak dependence, i.e., coefficient variation does not change the order of magnitude.

	T	z
a ₁	□	□
a ₂	□	□
a ₂₀	□	partially
B	□	partially
C	□	partially
D	partially	□
E	partially	□
F	partially	□
G	□	□
H	□	□

least to one parameter. Moreover, this preliminary study emphasizes the main issue related to bubble and dew problems with Bender NCEoS: in certain portions of the domain it is possible to achieve a negative pressure which pushes the NLS towards unfeasible solutions and the numerical solver is not able to recover and re-fall in the region even though constraints are set to the solver for the variables in question. This behaviour has been noted to be more common in case of dew problems as will be shown in the results section especially for temperatures close to triple and critical points. To avoid this unphysical behaviour a new algorithm is here proposed. According to the Bender thermodynamic model, the predicted pressure for a generic phase is defined as in (1)

$$P_{\text{EoS}}(T, d_m, z) = d_m T \left[R + \left(a_1 - \frac{a_2}{T} - B \right) d_m + Cd_m^2 + Dd_m^3 + Ed_m^4 + Fd_m^5 + (G + Hd_m^2)d_m^2 \cdot \exp(-a_{20}d_m^2) \right] \quad (1)$$

Omega term is defined as

$$\Omega(T, d_m, z) = R + \left(a_1 - \frac{a_2}{T} - B \right) d_m + Cd_m^2 + Dd_m^3 + Ed_m^4 + Fd_m^5 + (G + Hd_m^2)d_m^2 \cdot \exp(-a_{20}d_m^2) \quad (7)$$

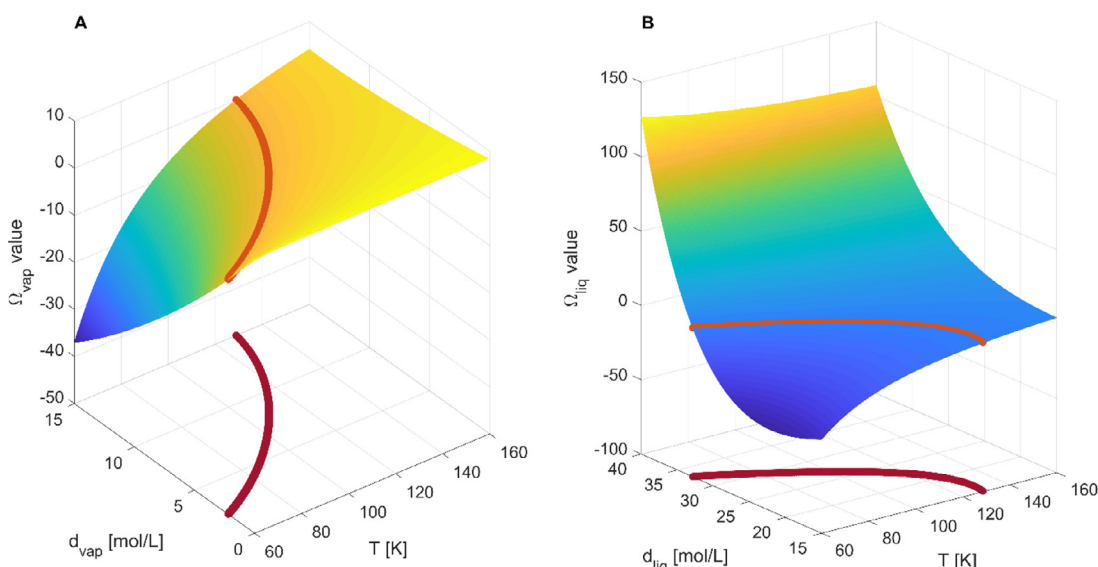


Fig. 3. Dry air omega function both for vapour (A) and liquid (B) phase.

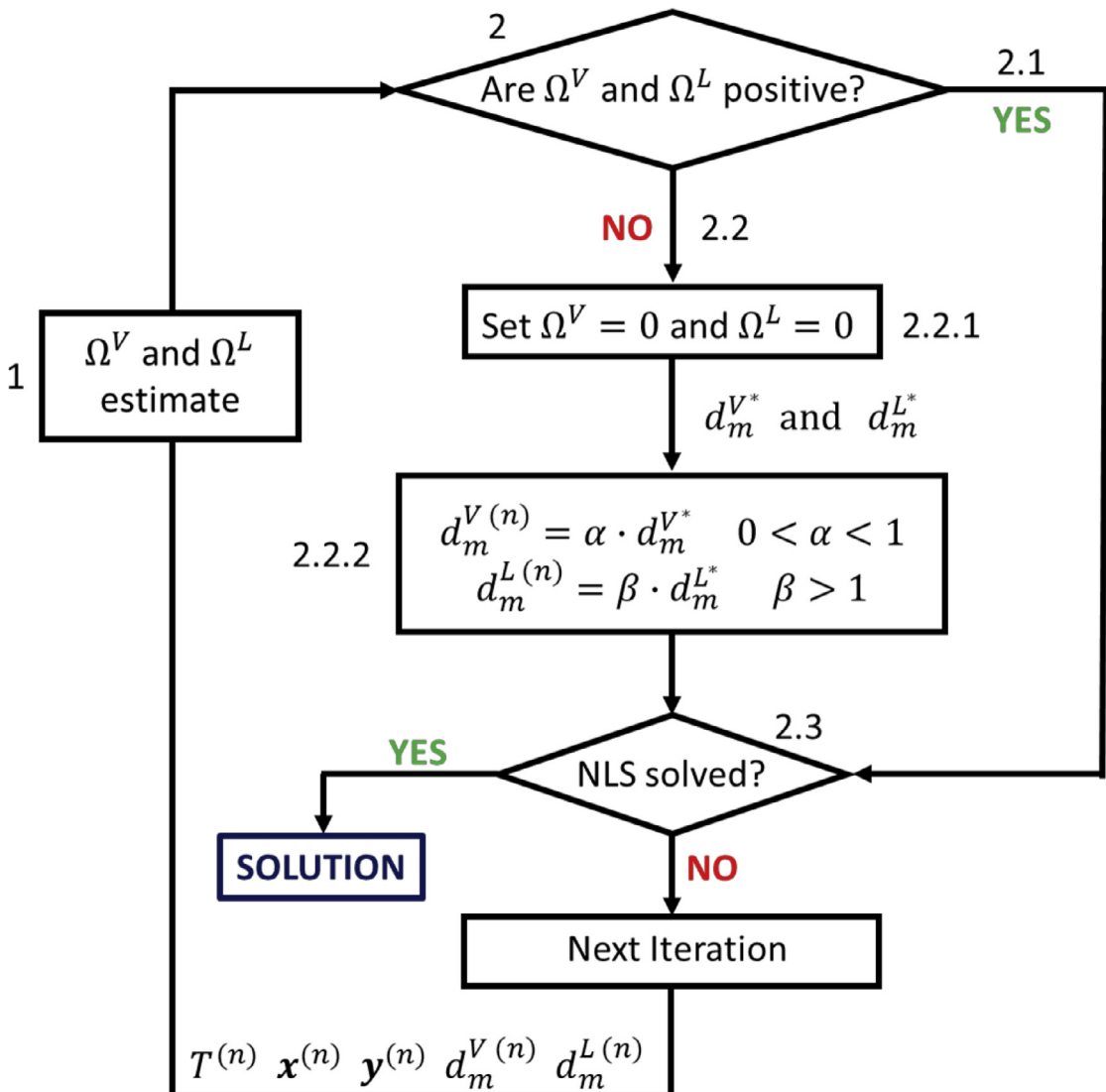


Fig. 4. Robust algorithm logical scheme for each NLS Solver Iteration.

[Eq. \(7\)](#) manages and determines the sign in [Eq. \(1\)](#). Therefore, major efforts should be focused on the general trend of the Omega function according to the phase involved (i.e., liquid and vapour). For more details, refer to Appendix D

As depicted in [Fig. 3](#), the Omega function, both for the liquid and vapour phases, can be split into two different regions: the positive and the negative one. These two regions are separated by the zeros level line (orange dots also called boundary line) whose projection is also drawn (dark red points). The Omega function resembles a constrained optimization problem with a fixed Pareto-front [58] which divides the feasible region (positive Omega function) from the unfeasible one, hence, the nonlinear system (NLS) can be solved as a constrained optimization problem [89]. However, in this case, a NLS solver has been used even though theoretically also a constrained optimization algorithm may be applied. To avoid any unfeasible behaviour of the nonlinear system, the phase density solution should be sought within the positive domain of the Omega function. At each iteration, the solver guessed solution is checked externally to prevent any issues and divergence from the feasible region:

Temporary composition, temperature, and phase density are exploited to evaluate the phase Omega function,

If the calculated point:

2.1 falls within the feasible region, the guessed values are kept and the NLS solver can perform the successive iteration;

2.2 on the contrary, the density value is modified according to (2.2.1 and 2.2.2)

2.2.1 keeping the parameters constant (pressure, temperature, and phase molar composition), it is possible to search for the molar density root such that the Omega function nullifies (i.e., move to one of dots along the orange line)

2.2.2 a temporary value is furtherly modified in order to move inside the feasible region: slightly increased for the liquid density and decreased for the vapor phase, as depicted in [Fig. 3](#).

2.3 solution check: if the NLS solver has not converged to a solution, the solver proceeds with a new iteration and the procedure restarts from step n.1, otherwise, the NLS has found the solution.

The procedure is illustrated in [Fig. 4](#).

Moreover, at each step, an additional hint to enhance the solver convergence has been deduced by looking at both the equilibrium equation and the Omega function shapes. From the NLS emerges that the constitutive law must be satisfied both for vapor and liquid phases. At the predicted equilibrium, the pressure is equal and uniform within the system, therefore, taking advantage of this physical

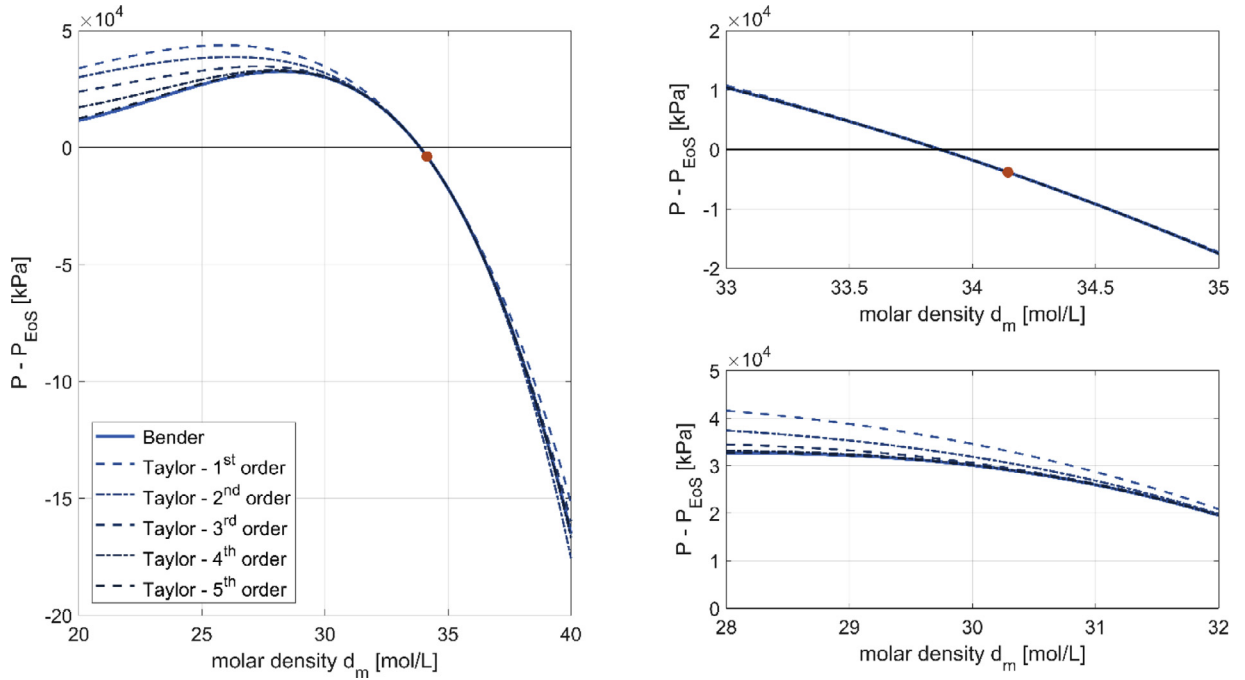


Fig. 5. Comparison between Bender function (solid blue line) and Taylor-expansion curve trends at different order: right-hand-side graphs show details of the overlapping between Bender function and fifth-order expansion model. Curves obtained for 85 K, 98 kPa, $z_{N_2} = 0.2089$ and $z_{O_2} = 0.6879$ and first-guess liquid density value $d_m^0 = 34.144 \text{ mol} \cdot \text{L}^{-1}$ (highlighted as an orange dot).

property, it is possible to combine Eq. 1 both for vapour and liquid phases obtaining:

$$d_m^V \cdot \Omega^V(T, d_m^V, y) - d_m^L \cdot \Omega^L(T, d_m^L, x) = 0 \quad (8)$$

Eq. (8) shows that the product between the phase density and its corresponding Omega function for both phases has to be equal. Hence, considering that

1. the molar density of the condensate phase is larger than the vapour one in order of magnitude,
2. the liquid phase Omega term increases its value for small density variation more rapidly than the vapour Omega term as clearly shown in Fig. 3 and Appendix D,

in order to fall inside the feasible domain, smart correction factors (i.e., α and β in Fig. 4) have been implemented to correct the phase density at each iteration. For the liquid, the proposed corrected density should stay very close to the boundary line, therefore the zero-line density is increased just for 1-3% of its value, while for the vapour phase a reduction of 5-10% has been used. The selection of the proper correction coefficients depends on temperature and pressure. In fact, discretizing the whole domain in temperature or pressure, the closer is the system to the critical point the lower will be the correction. In this way, the algorithm is able to properly work also closer to the critical point where vapor and liquid densities tend to coincide.

3.3. Efficient algorithm

The Robust algorithm ensures convergence and a reliable solution even though the computational effort and time are considerable. These last aspects are undesired disadvantages when a series of bubble/dew problems are to be solved repeatedly as in software for industrial applications, where accurate and fast results are needed. The convergence time may be reduced by partially modifying the original equations for pressure and the fugacity coefficients without losing robustness and numerical precision. The exponential parts in Eq. (1) and Eq. (2) significantly increase the nonlinearity and also the computational effort. In

order to remove these terms and speed up the calculation, it is worth applying a Taylor expansion around the first guess value for the phase density. According to the general Taylor expansion

$$f(x) = f(x_0) + \sum_n \frac{f^{(n)}(x_0)}{n!} (x - x_0)^n \quad (9)$$

The Taylor expansion has been applied on exponential term appearing in Eq. 1 and other terms and coefficients containing it (refer to Appendix B). The Taylor expansion is centred in the molar density (d_m^0) calculated from the Raoult problem as described in Section 3.1. The following derivatives are obtained:

$$f(d_m) = e^{-a_{20}d_m} \quad (10)$$

$$f^{(1)} = -2a_{20}d_m f(d_m) \quad (10.1)$$

$$f^{(2)} = 2a_{20}(2a_{20}d_m^2 - 1)f(d_m) \quad (10.2)$$

$$f^{(3)} = 4a_{20}^2(3d_m - 2a_{20}d_m^3)f(d_m) \quad (10.3)$$

$$f^{(4)} = 2a_{20}(3 - 12a_{20}d_m^2 + 4a_{20}^2d_m^4)f(d_m) \quad (10.4)$$

$$f^{(5)} = 8a_{20}^3d_m(-4a_{20}^2d_m^4 + 20a_{20}d_m^2 - 15)f(d_m) \quad (10.5)$$

The choice of expanding only around the molar density is due to the good accuracy of the first guess value for the phase molar density. Besides, the Taylor expansion has been stopped at the fifth-order because, as depicted in Fig. 5, the approximate curve tends to overlap to the original Bender NCEoS curve over quite a wide range and not only around the fixed point. Moreover, lower order-expansions show a certain discrepancy and therefore they do not guarantee convergence of the efficient algorithm.

The substitution of the exponential part with polynomial terms allows to furtherly simplify the shape of the equation and this results in faster and simpler convergence of the algorithm as shown in the results paragraph. The trade-off between computational speed and numerical accuracy is solved.

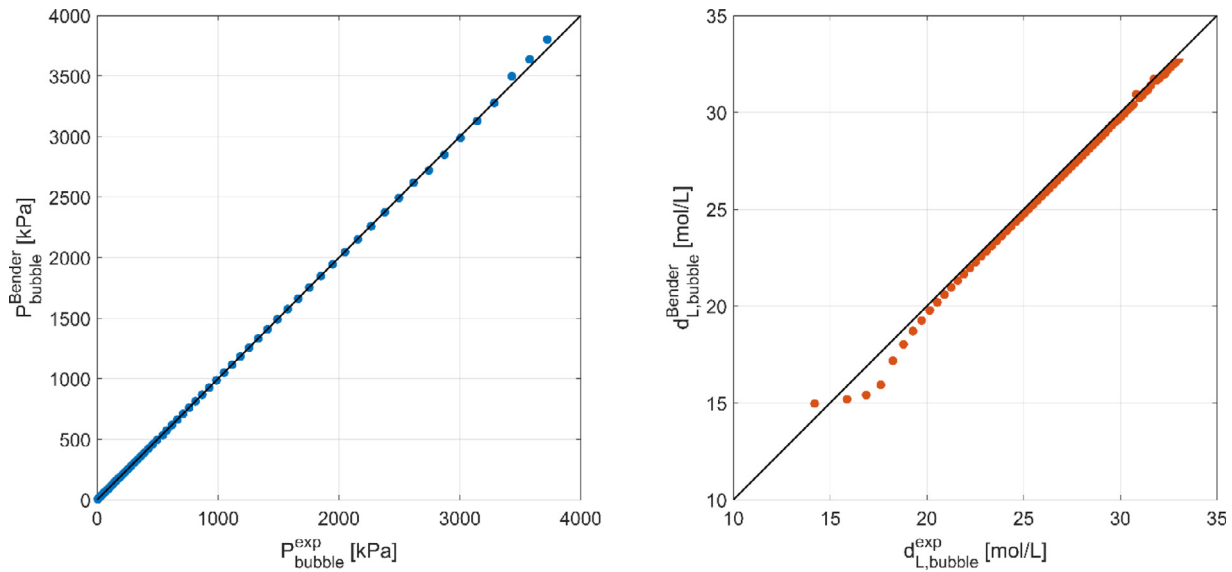


Fig. 6. Parity plots for predicted bubble pressure (left) and liquid density (right) with Bender model.

4. Case study and results

In this section, the performances of the different algorithms are compared both in terms of numerical accuracy and computational effort. It is worth testing and comparing the Bender EoS Efficient algorithm ([Section 3.3](#)) performance with respect to the most commonly used thermodynamic packages in Air Separation Unit [5], such as Peng-Robinson (PR), Soave-Redlich-Kwong (SRK), and Benedict-Webber-Rubin (BWR). For simplicity, bubble and dew problems in pressure are performed in the temperature range varying from 60 K up to 132 K for fixed dry air composition ($z_{N_2} = 0.7812$, $z_{O_2} = 0.2096$ and $z_{Ar} = 0.0092$). In the case of a bubble problem, the given composition corresponds to that of the liquid, while in the dew problem to that of the vapour phase. The reference data are directly taken from the NIST Database published in a specialized paper [48]. The NIST RefProp results for dry air has been considered as a reference since the authors claim that the relative errors for bubble/dew lines and relative phase density are lower than 0.1% between triple and critical points (the largest errors are close to the critical point, however, NIST model ensures that it does not exceed 0.1%). The NIST thermodynamic model results are listed in the appendix of the cited work and they are not reported in the present work. The Bender Equation of State has been implemented both in MatLab® environment and in Visual Studio C++ 2013 code where the BzzMath Library has been embodied [12], while concerning BWR, SRK and PR Equations of State thermodynamic packages in Aspen Hysys V10 have been used.

As a remark, in charts where the temperature is reported on the x-axis, vertical lines stand for the triple and critical temperatures.

The results section is subdivided into two different parts: (1) [Section 4.1](#) and [4.2](#) concern the bubble and dew problems respectively comparing the results for Bender's model with other CEoS and NCEoS while (2) [Section 4.3](#) shows the differences and main features for the different algorithms proposed in Methods and Algorithm paragraph.

4.1. Bubble problem

This paragraph reports the bubble problem results for dry air using the Efficient algorithm proposed in [Section 3.3](#). To compare the experimental data and the EoS results, parity graphs, and relative errors charts will be used. Although the pressure parity plot ([Fig. 6](#) left side) is intuitive, the molar density chart ([Fig. 6](#) right side) is slightly more complex: top-right corner is representative of points

close to the triple point, where, due to severe cryogenic conditions, the liquid phase is denser than in proximity of the critical point located in the bottom-left corner. The positions of the triple and critical point regions are exactly the opposite in the pressure parity chart. The relative error has been evaluated as:

$$\epsilon = \frac{y_{\text{exp}} - y_{\text{EoS}}}{y_{\text{exp}}} \quad (11)$$

Parity plot ([Fig. 6](#)) shows overlapping between the Bender model and experimental data. Specifically, the predicted bubble pressure is aligned with the experimental data, while the liquid density presents a deviation closer to the critical point as depicted also in [Fig. 9](#). However, [Fig. 7](#) proves that also the PR, SRK, and BWR liquid density predictions near the critical point deviate with respect to the experimental data while the Bender model performs better within this region. Moreover, the BWR model diverges in the proximity of the triple point, while the other thermodynamic models overlap perfectly with the experimental points.

The Bender model for the bubble pressure prediction, as already emphasized in [Fig. 6](#), agrees with experimental data. In detail, the Bender model gives better predictions near the triple point up to 80 K. However, the results provided by Bender and cubic EoS are comparable and similar along with the overall temperature range. The Bender relative error in pressure is generally within 1%, except for a few points. Worse performance is concentrated closer to the critical point where the relative error is still restrained but it increases up to almost 2% ([Fig. 8](#) right side). In any case, the full picture ([Fig. 8](#) left side) proves that BWR EoS is not a suitable thermodynamic tool to properly predict the bubble pressure for the air mixture. As a matter of fact, predictions are affected by a large relative error that continuously decreases up to the critical point.

Similarly, concerning the liquid phase density, the EoS provides good results, in particular, the Bender model relative error is always below 1.5% up to 125 K. All the analysed thermodynamic models worsen close to the critical points and the relative errors raise up to 20%. The Bender model profile is stable from 60 K up to 125 K and its trend is qualitatively in line the relative errors associated with other considered EoS: in this portion of the temperature domain, all the tested thermodynamic models exhibit smooth trends and great accuracy. For temperatures higher than 125 K (i.e., near the critical transition) Bender model shows a pick-trend, however, close to the critical point (i.e., 130 - 132 K) it ensures great accuracy, with a relative error

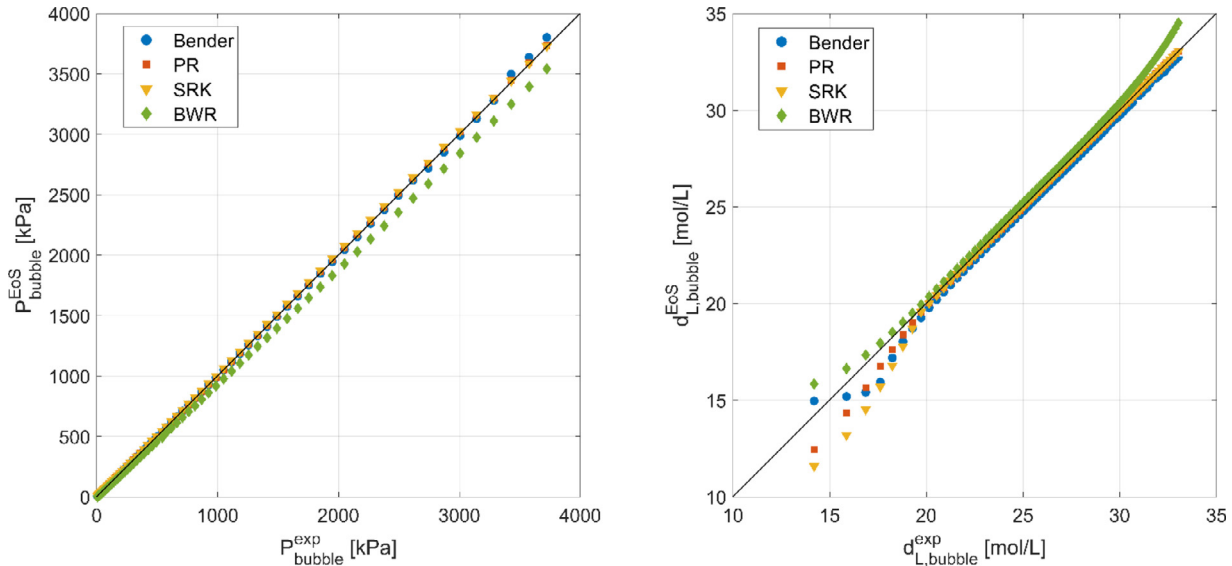


Fig. 7. Parity plot bubble pressure (left) and corresponding liquid density (right) predicted in temperature range 60K-132K by different EoS: Bender (blue), PR (red), SRK (yellow), and BWR (green). (For interpretation of the references to colour in this figure legend, the reader is referred to the web version of this article.)

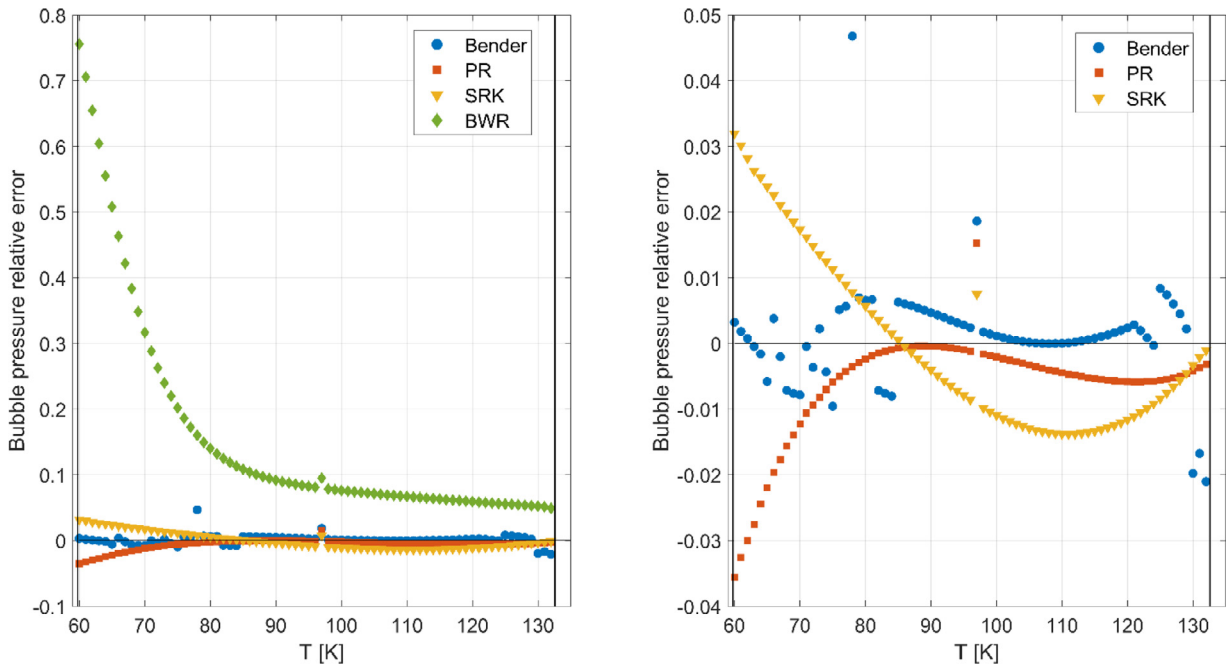


Fig. 8. Predicted bubble pressure relative error (left) and detail (right) with different EoS: Bender (blue), PR (red), SRK (yellow), and BWR (green). (For interpretation of the references to colour in this figure legend, the reader is referred to the web version of this article.)

below 5%, while PR, SRK, and BWR tends to diverge. Specifically, CEoS provides results affected by relative errors larger than 10%, as shown in Fig. 9.

4.2. Dew Problem

Parity plot (Fig. 10) proves an agreement between the dew pressure prediction and the experimental data, but for the vapour density chart, there is a slight deviation from the bisector close to the triple point. Qualitatively, the same trends are depicted in Fig. 11, where all the EoS show a discrepancy approaching the triple point except the Bender and SRK models that do not appear to suffer from this issue. Finally, all the considered EoS look to properly predict and describe the mixture properties close to the critical point.

Previous considerations are confirmed in Figs. 12 and 13. BWR seems not to be a suitable thermodynamic model to solve the dew problem for the air mixture. Moreover, it is possible to claim that all the EoS show worsened performances when compared to the bubble problem. Specifically, the Bender's model relative error increases up to 3% for the majority of the case studies but there are some points where relative errors reach 9%. Close to the critical point, the Bender model returns providing accurate results and the relative error is kept below 4% and comparable to that of the CEoS.

Concerning the vapour phase density, the Bender model exhibits a good agreement with respect to the RepProp package developed by NIST. The relative error is kept within $\pm 5\%$ except for few cases mainly concentrated close to the critical point. However, in this region, the largest relative error is almost 7%. In addition, as

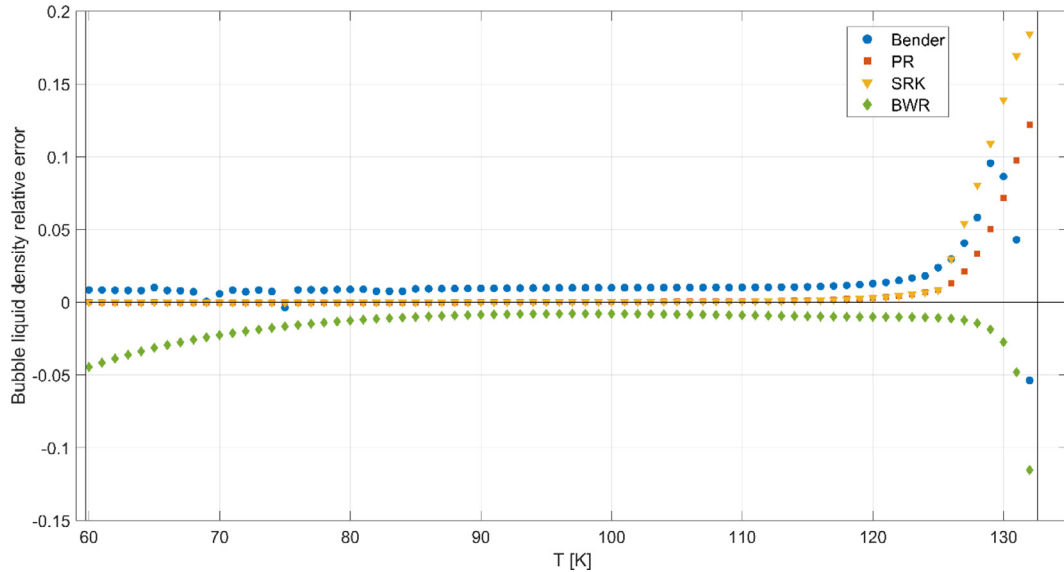


Fig. 9. Predicted liquid density relative error at different temperatures (from 60 K up to 132 K) with different EoS: Bender (blue), PR (red), SRK (yellow), and BWR (green). (For interpretation of the references to colour in this figure legend, the reader is referred to the web version of this article.)

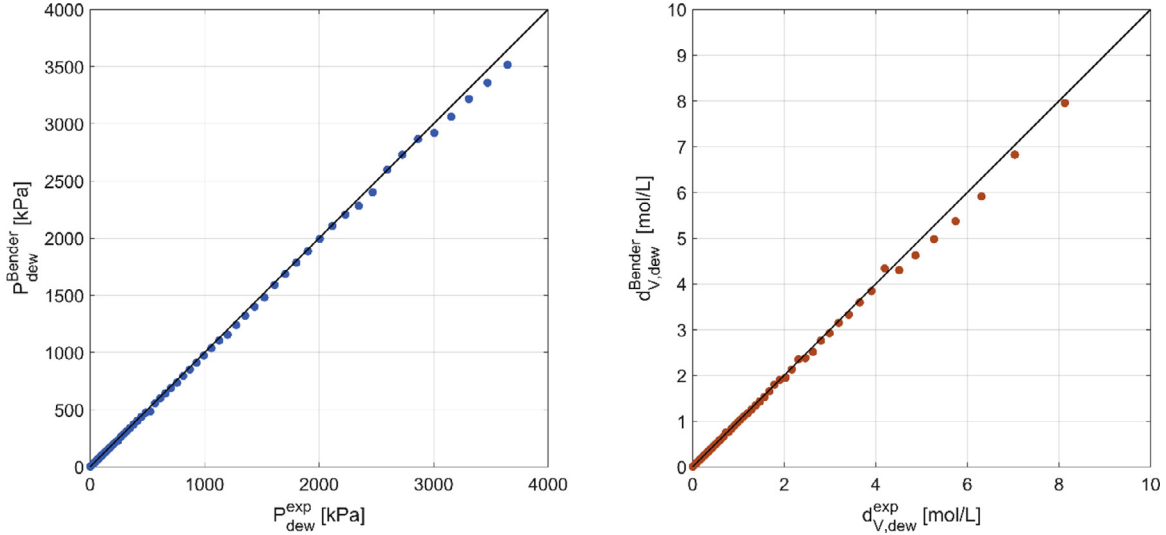


Fig. 10. Parity plots for predicted dew pressure (left) and vapour density (right) with Bender model.

confirmed in parity plot in Fig. 10, the Bender model seems to underestimate the corresponding vapour molar density. PR EoS shows a parabolic shape in errors trends, indeed, it appears inaccurate close to both critical and triple points (relative error larger close to 10%), while qualitatively it overlaps to experimental points in the range of 85 – 110 K. SRK is still the EoS that better predicts mixture properties in the dew problem for dry air even when approaching the critical point. SRK's model results are comparable to those obtained with the Bender NCEoS applying the Efficient algorithm.

4.3. Comparison of the Bender solution algorithms

In this paragraph, the algorithms presented in Section 3 are compared in terms of accuracy and computational time. The dry air bubble and dew problems are still used as a reference case study to compare performances and accuracy.

4.3.1. Bubble problem accuracy

Figs. 14 and 15 clearly prove that the Standard algorithm (Section 3.1) is not sufficient to handle bubble problems with the Bender

EoS. Moreover, sometimes this algorithm is not able to converge to a solution or it may even provide results that are not the real solution of the system. These points are denoted with 100% relative error and they are concentrated in proximity of triple and critical points. Robust and Efficient strategies provide results within 5% of error in pressure and liquid density (except for few points close to the critical point where error raises to almost 10%). More in general, the Efficient algorithm presents relative errors which are distributed around a mean value of 0.5% and the relative error is kept below 1%. Both Robust and Efficient algorithms exhibit spikes or errors moving towards the critical point: the error is kept below 3.5% in the case of pressure while it slightly increases up to 9% for liquid density predictions. The Robust algorithm shows also a second spike in relative error in bubble pressure prediction in the proximity of the triple point (60 – 65 K), however, the relative error is always lower than 4%.

4.3.2. Dew problem accuracy

Concerning the dew problem, Fig. 16 demonstrates that the Standard algorithm is not able to solve the problem and only Robust and Efficient algorithms provide a numerical solution. The accuracy of

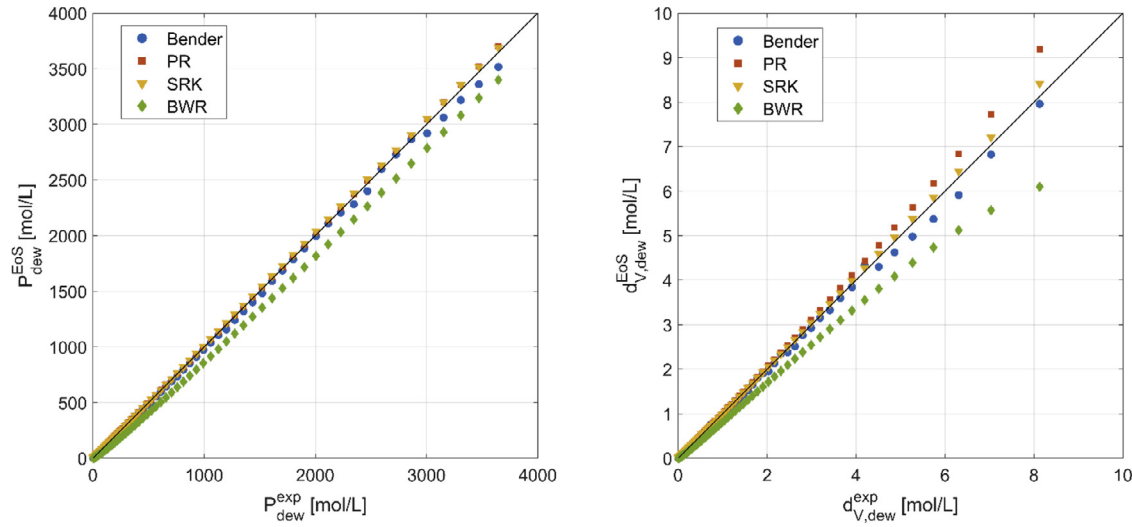


Fig. 11. Parity plot dew pressure (left) and corresponding vapour density (right) predicted in the temperature range 60 K - 132 K by different EoS: Bender (blue), PR (red), SRK (yellow), and BWR (green). (For interpretation of the references to colour in this figure legend, the reader is referred to the web version of this article.)

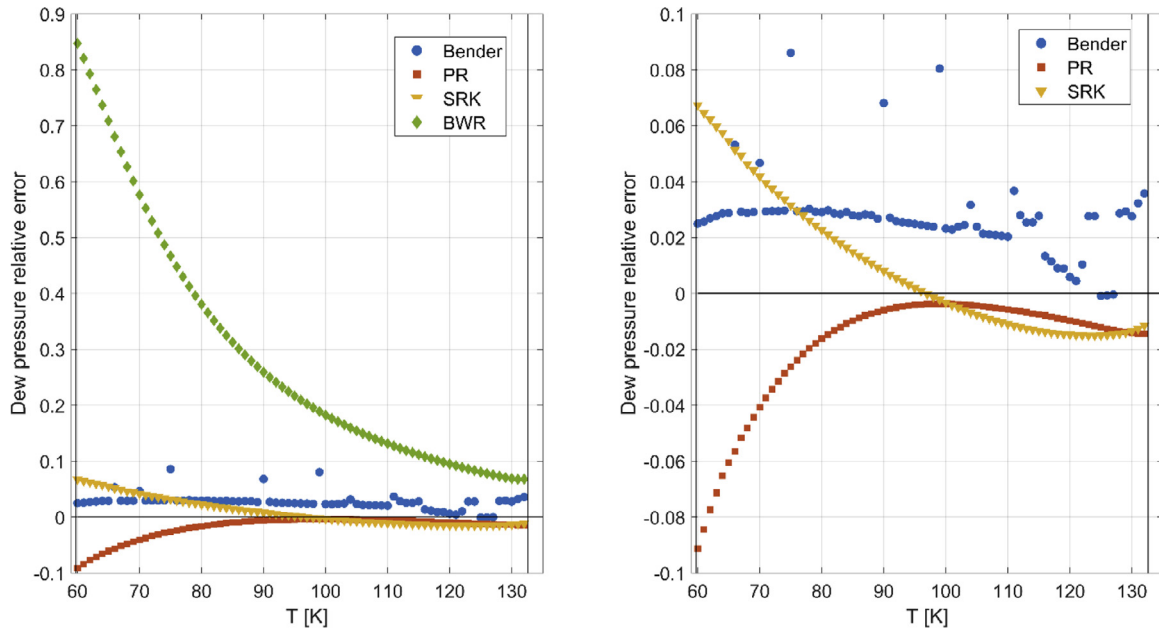


Fig. 12. Predicted dew pressure relative error (left) and detail (right) with different EoS: Bender (blue), PR (red), SRK (yellow), and BWR (green). (For interpretation of the references to colour in this figure legend, the reader is referred to the web version of this article.)

both is similar, but, as already underlined in paragraph 3.2, the accuracy is worsened in the dew problem, and the efficient algorithm guarantees errors within 8% error margin for pressure and 7% for density. Moreover, Fig. 16 proves the issue presented in Section 3.2: in the Standard Algorithm for the dew problem, the numerical solver is not able to ensure a physically acceptable solution and it falls in the infeasible region providing a negative pressure as a result. Since the solver violates physical constraints, the unfeasible results have been considered null and consequently, the relative error is 100%. The same issue is present for the bubble problem, but it is less frequent (Fig. 15). As depicted in Fig. 17, just focusing on Robust and Efficient algorithms, it is possible to highlight that the Efficient algorithm tends to keep the relative errors distributed around an average value (2%), while the Robust algorithm exhibits a decreasing trend. However, larger errors are localised around the triple point (>20%) and the critical point (>15%). This proves that the Efficient algorithm effectively enables to mitigate the presence of large errors close to the upper and lower limits of the temperature domain, while, in the

middle range (80 - 120 K) errors are kept similar (below 2.5%) to the ones of Robust method despite it generally performs better.

4.3.3. Computational time

Accuracy, efficiency, and computational efforts are key parameters to evaluate the performances and robustness of algorithms [11,12,57]. In this paragraph, the computational time of the three proposed numerical strategies will be analysed in order to identify whether the Efficient algorithm (paragraph 3.3) is an effective enhancement of the Robust one (paragraph 3.2). Fig. 18 and Table 2 prove that both for dew and bubble problems, the computational time has been drastically reduced: the Efficient algorithm ensures convergence, as already discussed, and additionally, it reduces the computational time within the VLE domain including the points close to the triple and critical points. The computational time requested by the Robust algorithm (square markers in Fig. 18) is generally lower than the Standard algorithm (circle markers). The Standard algorithm computational times are more oscillating: as a general consideration,

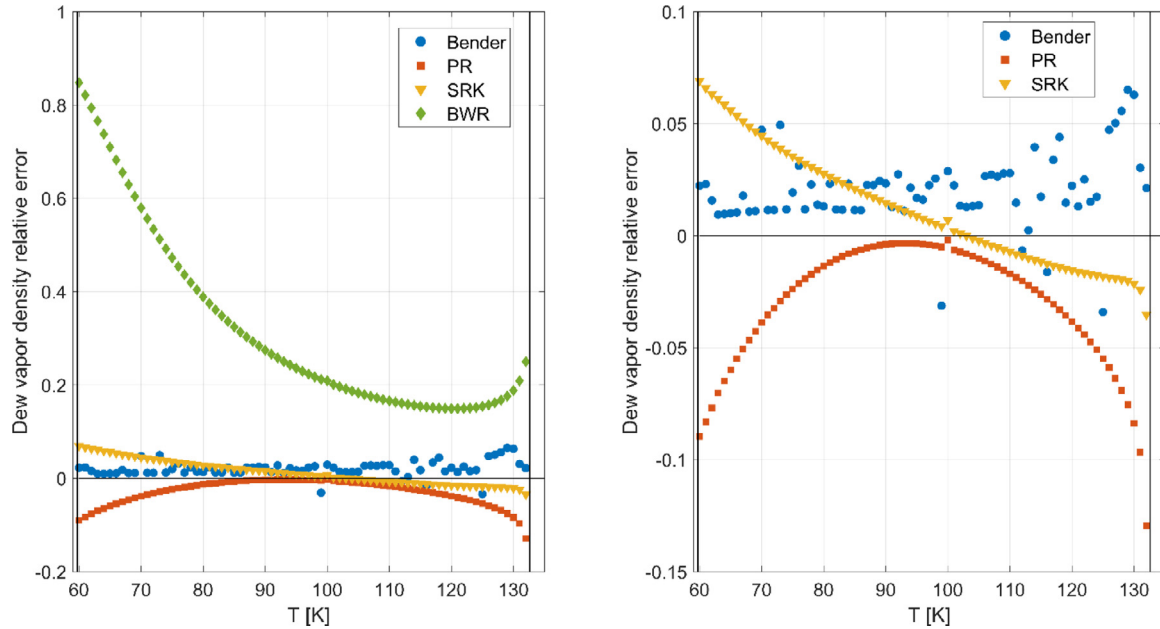


Fig. 13. Predicted liquid density relative error at different temperatures (from 60 K up to 132 K) with different EoS: Bender (blue), PR (red), SRK (yellow), and BWR (green). On the right side, a detail focusing on the Bender model and CEoS. (For interpretation of the references to colour in this figure legend, the reader is referred to the web version of this article.)

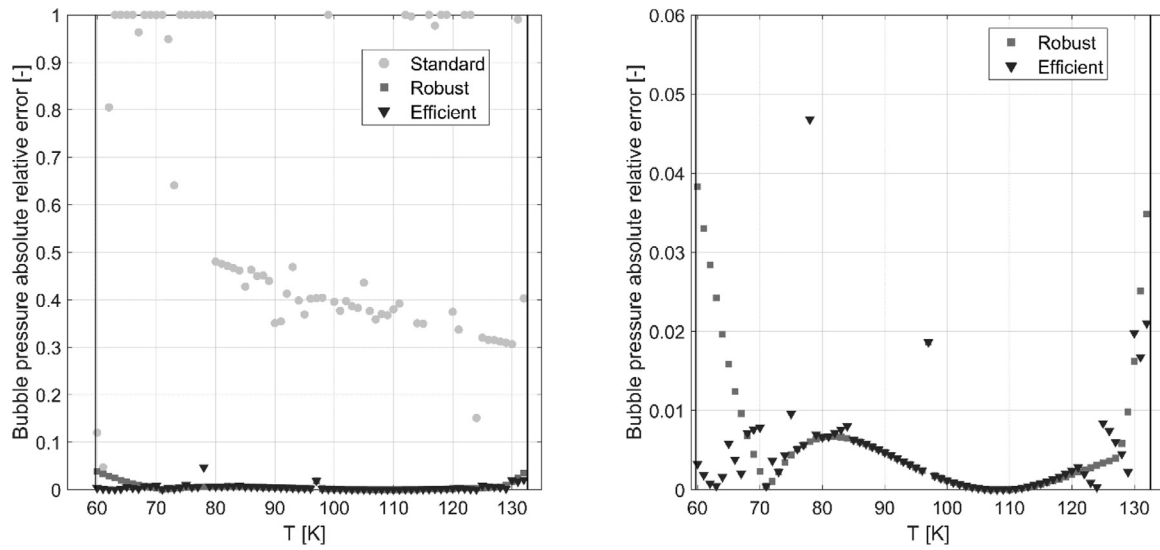


Fig. 14. Bender solution algorithms comparison: bubble pressure relative error.

this algorithm requires more time to converge to a solution, if it converges in the first place. For temperatures higher than 110 K in the bubble problem, the Standard algorithm performances seem to be promising, however, this trend is completely misleading since looking at Fig. 16 it appears that the results are affected by large errors (>15%). Moreover, since the Standard algorithm is not suitable to solve the dew problem, in Fig. 18 the right-hand-side circle markers are not present. Considering the Robust algorithm, square markers look clustered which means that the algorithm is strongly affected by the operating condition. Time data clustering is more evident for the dew problem (Fig. 18 left-hand-side) where the Robust algorithm slowly converges to a numerical solution closer to the critical point and for temperatures higher than 100 K. Still focusing on this temperature range (i.e 120 - 132 K), the computational time shows an average increasing linear trend. As a matter of fact, the Robust algorithm allows to solve bubble and dew problems with good numerical accuracy (Fig. 16 and 17), however, it is not fully stable since

computational time depends on the operating condition and this behavior is magnified according to which problem should be solved. For instance, the bubble problem requires, on average 331 ms, while the dew problem 836 ms. This discrepancy is not evident for the Efficient algorithm (triangular markers): 66 ms for bubble problem and 90 ms for the dew one. Moreover, the Efficient algorithm does not exhibit any data clustering, indeed, computational times are distributed around the average value. Similar considerations may be proposed for numerical accuracy. As reported in Table 2, the relative error trends show a strong reduction meaning that both Robust and Efficient algorithms produce an improvement in the numerical accuracy with respect to the Standard one. Comparing these two algorithms, it is possible to state that the Taylor expansion benefits on average computational time and relative error. This effect is more evident in the dew problem. The main difference between Robust and Efficient algorithms lies in computational time. As already discussed, the Efficient algorithm causes an effective reduction of the

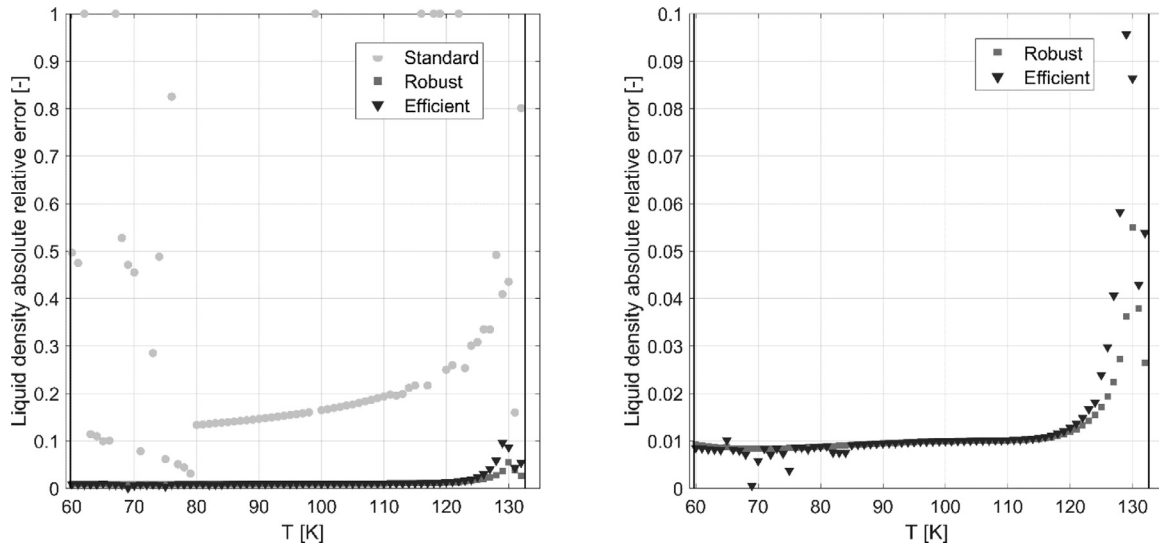


Fig. 15. Bender solution algorithms comparison: liquid density relative error.

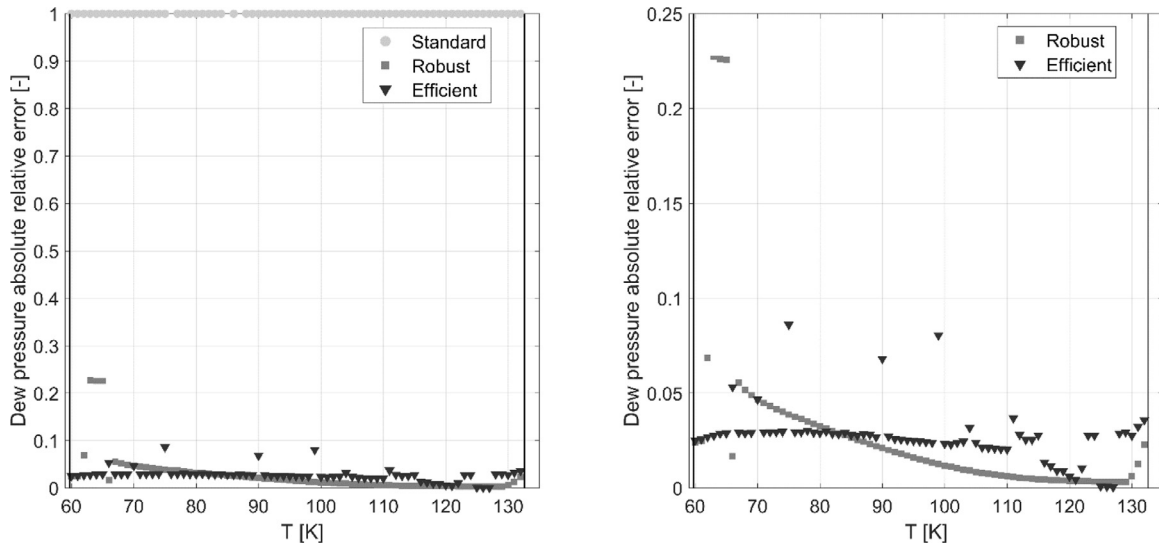


Fig. 16. Bender solution algorithms comparison: dew pressure (left) and liquid density (right) relative errors.

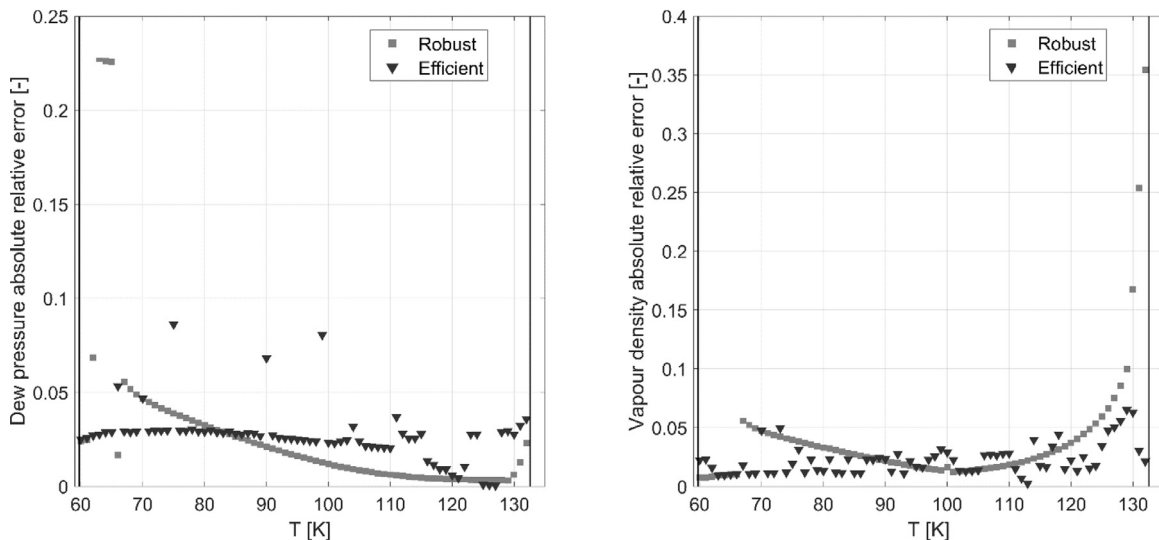


Fig. 17. Comparison of relative errors for robust and efficient algorithms in dew problem.

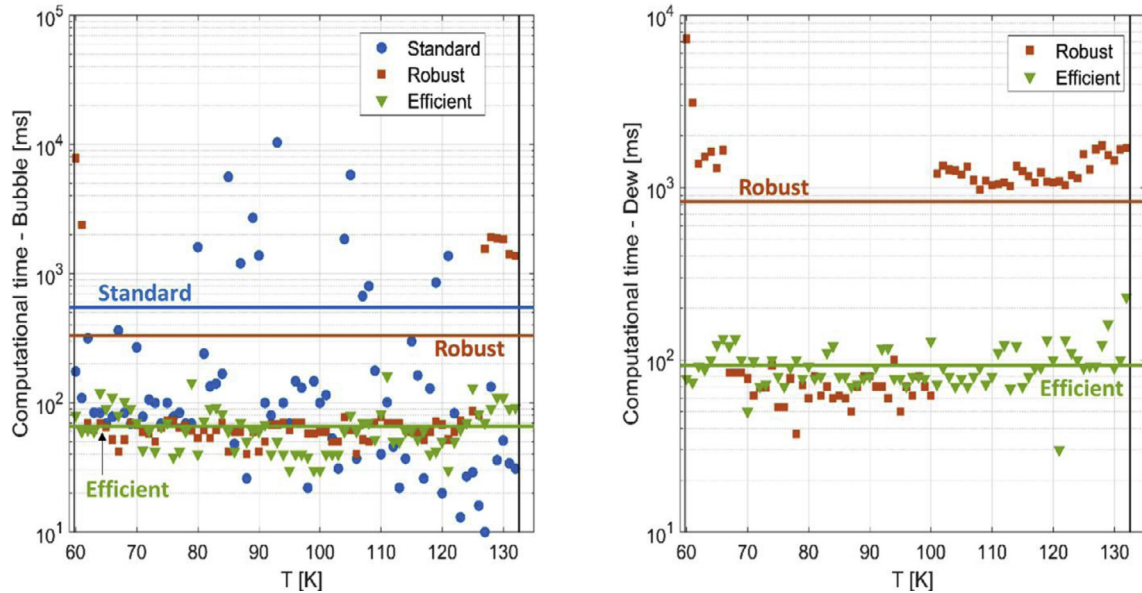


Fig. 18. Standard (blue), Robust (red), and Efficient (green) algorithms computational time. The corresponding horizontal lines are the average computational time for each proposed algorithm. (For interpretation of the references to colour in this figure legend, the reader is referred to the web version of this article.)

Table 2

Comparison of algorithms performances.

Algorithm	Bubble problem			Dew problem		
	ε_p [%]	ε_d [%]	t [ms]	ε_p [%]	ε_d [%]	t [ms]
Standard	60.4	30.2	549	-	-	-
Robust	0.63	1.20	331	2.76	3.91	826
Efficient	0.47	1.44	66	2.71	2.24	90

computational time. The impact is reflected in a reduction of one order of magnitude as reported in **Table 2**. For the bubble problem, the computational time becomes five times lower whereas for the dew problem almost ten times.

5. Conclusions

In air separation units (ASU), severe cryogenic conditions require reliable equations of state (EoS) to accurately predict the thermodynamic behavior of the ternary mixture. It has been proved that the Bender model is a suitable thermodynamic tool able to properly describe the mixture properties in vapour-liquid equilibria in the cryogenic environment. In fact, the results provided are comparable to that of industrially validated and more commonly used Peng-Robinsons (PR) and Soave-Redlich-Kwong (SRK) EoS. Despite some criticisms and warnings [41], these preliminaries are encouraging and seem to open a perspective to implement the Bender non-cubic equation of state (NCEoS) for industrial applications in the ASU field. Moreover, three different algorithms have been developed and proposed to overcome numerical and intrinsic issues due to the NCEoS formulation. The efficient algorithm is a trade-off between numerical accuracy and computational time and effort required. Finally, since the general approach proposed in Bender's work [5] has also been applied recently for several additional compounds, the algorithms here discussed can be easily transferred to these species and they may also be exploited as a general strategy for the solution of bubble and dew problems using NCEoS other than the Bender model.

Declaration of Competing Interest

None.

Appendix

Appendix A. – Bender Equation of State coefficients and mixing rules

In this appendix, twenty pure components coefficients and the mixing rules both for pressure [Eq. \(1\)](#) and fugacity coefficient [Eq. \(2\)](#) are provided. Moreover, since in Bender's works [5], units of measure are missing and sometimes not consistent, the correct units of measure are listed in [Table A.1](#). For more details on the implementation of vector and matrix products to evaluate the mixing coefficients, see the cited reference [8].

In order to be consistent with the twenty coefficients provided in [5] and reported in [Table A.2](#), the following units of measurement should be used although Bender himself suggested several wrong ones [5,6].

Coefficients gathered in [Table A.2](#) are necessary to evaluate coefficients appearing in [Eqs. \(1\)](#) and [\(3\)](#). Some preliminary calculations are necessary:

Table A.1
Units of measure to be adopted with Bender EoS.

Variable	Unit of Measure
Pressure – P	[kPa]
Temperature – T	[K]
Molar density – d_m	[mol/L]
Gas Constant – R	[kPa·L/(mol·K)]

Table A.2
Pure compound coefficients ($a_{i,k}$).

i	Nitrogen ($k = 1$)	Argon ($k = 2$)	Oxygen ($k = 3$)
1	0.37713681	0.31639051	0.35643862
2	$0.11808150 \cdot 10^3$	$0.13043320 \cdot 10^3$	$0.14407294 \cdot 10^3$
3	$-0.20459519 \cdot 10^4$	$-0.28370046 \cdot 10^4$	$-0.25661301 \cdot 10^4$
4	$0.10039112 \cdot 10^7$	$0.13150788 \cdot 10^7$	$0.10322523 \cdot 10^7$
5	$-0.23100097 \cdot 10^8$	$-0.50534111 \cdot 10^8$	$-0.19530479 \cdot 10^8$
6	$0.82438827 \cdot 10^{-2}$	$-0.28179523 \cdot 10^{-2}$	$0.13149946 \cdot 10^{-3}$
7	$-0.11154107 \cdot 10^1$	$0.39628356 \cdot 10^1$	$0.21353195 \cdot 10^1$
8	$0.31874442 \cdot 10^3$	$0.72951535 \cdot 10^3$	$0.35916916 \cdot 10^3$

(continued)

Table A.2 (Continued)

<i>i</i>	Nitrogen (<i>k</i> = 1)	Argon (<i>k</i> = 2)	Oxygen (<i>k</i> = 3)
9	$0.88741591 \cdot 10^{-3}$	$0.1217661 \cdot 10^{-2}$	$0.73097410 \cdot 10^{-3}$
10	-0.14864235	-0.50030773	-0.27513075
11	$0.499951582 \cdot 10^{-5}$	$-0.21947285 \cdot 10^{-4}$	$0.64203761 \cdot 10^{-5}$
12	-0.47638192 $\cdot 10^{-3}$	$0.16831369 \cdot 10^{-1}$	$0.98687798 \cdot 10^{-3}$
13	$0.17421249 \cdot 10^{-3}$	$-0.11437390 \cdot 10^{-3}$	$0.84733604 \cdot 10^{-4}$
14	-0.44153012 $\cdot 10^5$	$0.52614785 \cdot 10^4$	$-0.63010952 \cdot 10^5$
15	$0.95112155 \cdot 10^7$	$-0.58356378 \cdot 10^6$	$0.15107048 \cdot 10^8$
16	-0.36302552 $\cdot 10^9$	$-0.11692362 \cdot 10^9$	$-0.13084843 \cdot 10^{10}$
17	-0.17495594 $\cdot 10^3$	$-0.34445957 \cdot 10^3$	$-0.19018424 \cdot 10^3$
18	$0.81455788 \cdot 10^5$	$0.15802557 \cdot 10^6$	$0.45774043 \cdot 10^5$
19	-0.20730231 $\cdot 10^7$	$-0.68651100 \cdot 10^7$	$0.30856640 \cdot 10^7$
20	$0.78475058 \cdot 10^{-2}$	$0.55854495 \cdot 10^{-2}$	$0.55291853 \cdot 10^{-2}$

$$B_k = \frac{a_{3,k}}{T^2} + \frac{a_{4,k}}{T^3} + \frac{a_{5,k}}{T^4} \quad (\text{A.1})$$

$$C_k = a_{6,k} + \frac{a_{7,k}}{T} + \frac{a_{8,k}}{T^2} \quad (\text{A.2})$$

$$D_k = a_{9,k} + \frac{a_{10,k}}{T} \quad (\text{A.3})$$

$$E_k = a_{11,k} + \frac{a_{12,k}}{T} \quad (\text{A.4})$$

$$F_k = \frac{a_{13,k}}{T} \quad (\text{A.5})$$

$$G_k = \frac{a_{14,k}}{T^3} + \frac{a_{15,k}}{T^4} + \frac{a_{16,k}}{T^5} \quad (\text{A.6})$$

$$H_k = \frac{a_{17,k}}{T^3} + \frac{a_{18,k}}{T^4} + \frac{a_{19,k}}{T^5} \quad (\text{A.7})$$

Pressure coefficients

By indicating parameters (A.1) – (A.7) as generic Y_k parameters, mixing rules for coefficients (generically denoted as Y) in Eq. (1) are provided. In particular for:

- coefficients a_2, B and a_{20} geometrical mixing rule is applied

$$Y = \left(\sum_{k=1}^3 z_k Y_k^{1/2} \right)^2 \quad (\text{A.8})$$

- coefficient C cubic mixing rule is suggested

$$Y = \left(\sum_{k=1}^3 z_k Y_k^{1/3} \right)^3 \quad (\text{A.9})$$

- all other coefficients linear mixing rule is provided

$$Y = \sum_{k=1}^3 z_k Y_k \quad (\text{A.10})$$

$$a_1 = \sum_{k=1}^3 z_k a_{1,k} \quad (\text{A.11})$$

$$a_2 = \left(\sum_{k=1}^3 z_k \sqrt{a_{2,k}} \right)^2 \quad (\text{A.12})$$

$$B = \left(\sum_{k=1}^3 z_k \sqrt{B_k} \right)^2 \quad (\text{A.13})$$

$$C = \left(\sum_{k=1}^3 z_k 3\sqrt{C_k} \right)^3 \quad (\text{A.14})$$

$$D = \sum_{k=1}^3 z_k D_k \quad (\text{A.15})$$

$$E = \sum_{k=1}^3 z_k E_k \quad (\text{A.16})$$

$$F = \sum_{k=1}^3 z_k F_k \quad (\text{A.17})$$

$$H = \sum_{k=1}^3 z_k H_k \quad (\text{A.18})$$

$$a_{20} = \left(\sum_{k=1}^3 z_k \sqrt{a_{20,k}} \right)^2 \quad (\text{A.19})$$

The only exception to standard mixing rules is given by G mixing parameter. Bender found out that the linear mixing rule alone was not correct due to binary mixtures deviations. The additional term in the mixing rule, therefore, accounts for these deviations and it is the result of nonlinear regression on experimental data sets:

$$G = \sum_{k=1}^3 z_k G_k + \sum_{i=1}^3 \sum_{j=i+1}^3 \left[\alpha_{ij} \left(\frac{100}{T} \right)^{m_{ij}} + \beta_{ij} \right] z_i z_j \quad (\text{A.20})$$

Values of the parameters α_{ij} , β_{ij} and m_{ij} are provided in matrix form

$$\alpha_{ij} = \begin{bmatrix} 0 & -0.0072 & 0.0057 \\ -0.0072 & 0 & 0.0095 \\ 0.0057 & 0.0095 & 0 \end{bmatrix} \quad (\text{A.21.1})$$

$$\beta_{ij} = \begin{bmatrix} 0 & 0.007 & 0 \\ 0.007 & 0 & 0.004 \\ 0 & 0.004 & 0 \end{bmatrix} \quad (\text{A.21.2})$$

$$m_{ij} = \begin{bmatrix} 0 & 6 & 8 \\ 6 & 0 & 4 \\ 8 & 4 & 0 \end{bmatrix} \quad (\text{A.21.3})$$

Fugacity coefficients

Similarly, here coefficients appearing in Eq. (3) are provided. In each term, it is possible to partially recognize mixing coefficients (A.11) – (A.19)

$$a_1^F = \sum_{k=1}^3 z_k a_{1,k} + a_{1,k} \quad (\text{A.22})$$

$$a_2^F = \left(\sum_{k=1}^3 z_k a_{1,k}^{1/2} \right) \cdot a_{1,k}^{1/2} \quad (\text{A.23})$$

$$B_F = \left(\sum_{k=1}^3 z_k B_k^{1/2} \right) \cdot B_k^{1/2} \quad (\text{A.24})$$

$$C_F = \left(\sum_{k=1}^3 z_k C_k^{1/3} \right)^2 \cdot C_k^{1/3} \quad (\text{A.25})$$

$$D_F = \sum_{k=1}^3 z_k D_k + \frac{D_k}{3} \quad (\text{A.26})$$

$$E_F = \sum_{k=1}^3 z_k E_k + \frac{E_k}{4} \quad (\text{A.27})$$

$$F_F = \sum_{k=1}^3 z_k F_k + \frac{F_k}{5} \quad (\text{A.28})$$

$$H_F = 4 \left(\sum_{k=1}^3 z_k H_k \right) + H_k \quad (\text{A.29})$$

While parameter G_F has slightly more complex expression that depends on the considered specie

$$G_F^{k=1} = 2G + G_k + \left\{ \left[-0.0072 \left(\frac{100}{T} \right)^6 + 0.007 \right] z_2(1-z_1) + 0.0057 \left(\frac{100}{T} \right)^8 z_3(1-z_1) \right\} \quad (\text{A.30.1})$$

$$\text{scale80\%} G_F^{k=2} = 2G + G_k + \left\{ \left[-0.0072 \left(\frac{100}{T} \right)^6 + 0.007 \right] z_1(1-z_2) + \left[0.0095 \left(\frac{100}{T} \right)^4 + 0.004 \right] z_3(1-z_2) \right\} \quad (\text{A.30.2})$$

$$G_F^{k=3} = 2G + G_k + \left\{ 0.0057 \left(\frac{100}{T} \right)^8 z_1(1-z_3) + \left[0.0095 \left(\frac{100}{T} \right)^4 + 0.004 \right] z_2(1-z_3) \right\} \quad (\text{A.30.3})$$

Finally

$$\beta_1 = \frac{G_F + H_F/a_{20}}{2a_{20}d_m^2} \quad (\text{A.31})$$

$$\beta_2 = \exp(-a_{20}d_m^2) \left[\frac{G_F}{2a_{20}d_m^2} + \frac{H_F}{2a_{20}} \left(1 + \frac{1}{a_{20}d_m^2} \right) \right] \quad (\text{A.32})$$

$$\beta_3 = \frac{G}{a_{20}d_m^2} [1 - \exp(-a_{20}d_m^2) \cdot (a_{20}d_m^2 + 1)] \quad (\text{A.33})$$

$$\beta_4 = \frac{H}{(a_{20}d_m)^2} \left\{ 2 - \exp(-a_{20}d_m^2) \cdot [(a_{20}d_m^2 + 1)^2 + 1] \right\} \quad (\text{A.34})$$

It is fundamental to emphasize that for a single-phase (i.e., only liquid, only vapour, or supercritical fluid), the elements (A.11) – (A.20) are numbers, while all parameters are defined in (A.22) – (A.34) are vectors. In the case of vapour-liquid equilibria, the firsts become vectors instead of the latter matrixes. Moreover, it is worth taking advantage of the vector-matrix product to speed up calculations [8].

Appendix B. – Sensitivity analysis on coefficients

A sensitivity analysis has been performed on the mixing coefficient of the Bender EoS (A.11) – (A.20). By fixing the temperature, the phase composition is the only adjustable variable. Since

air is a ternary mixture, only nitrogen and argon composition (x_1 and x_2 respectively) are shown, considering that the composition in oxygen must satisfy the normalized stoichiometry sum. In order to avoid useless calculations, the unfeasible domain, where the sum of x_1 and x_2 is larger than the unit (i.e., the point along the diagonal of the square defined by the molar fraction axes and the associated area), has been automatically removed. Temperatures have been selected in order to cover the whole domain where vapor-liquid is possible, hence, from the triple point up to the critical point. The following 3D-plots are representative of

60K (a), 90K (b), and 120K (c). In the same cases, x and y axes orientation is changed in order to have a better view of the curves disposition in the space.

Table B.1 lists the maximum and minimum value of each mixing coefficient at 60 K, 90 K, and 120 K. From **Table B.1** it is possible to appreciate the order of magnitude associated with the mixing coefficients and the impact of temperature on their value. For the sake of completeness, **Figs. B.11 and B.12** graphically show the percentage variation of maximum and minimum respectively within the typical operating condition for air cryogenic separation (60 – 120 K). Since mixing coefficients $a_{1\text{mix}}$, $a_{2\text{mix}}$ and $a_{20\text{mix}}$ are not sensible to temperature, their variation is not plotted in the charts. In the charts, the parameters percentage variations have been estimated considering as reference the values at 60 K:

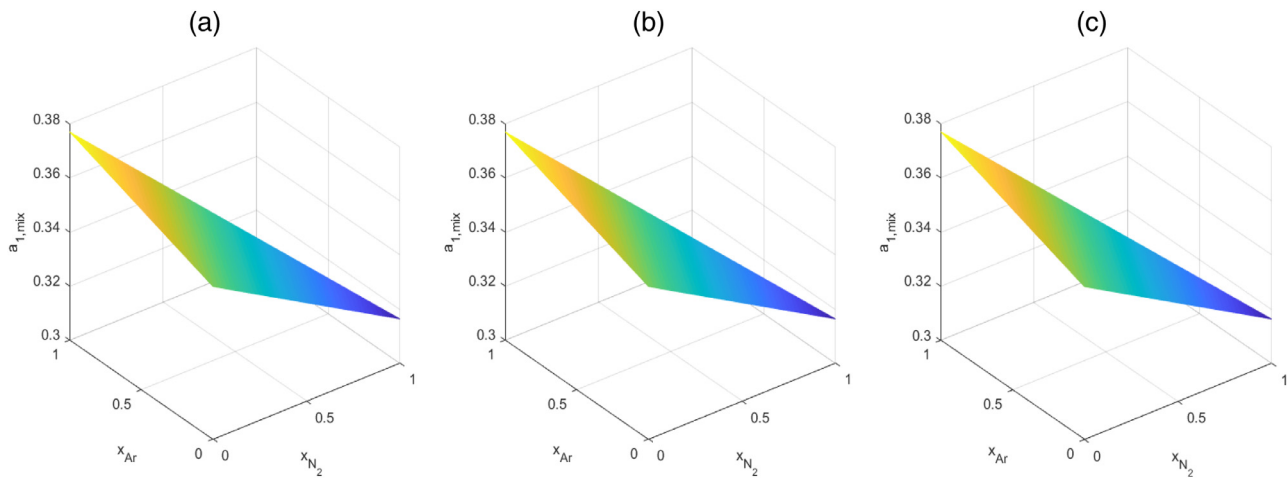
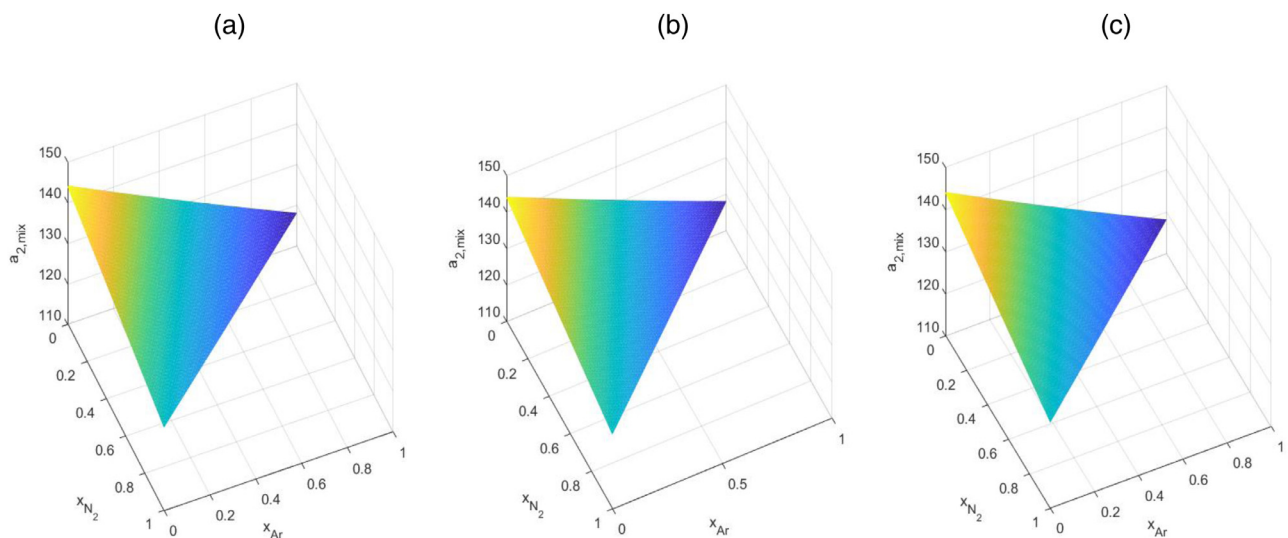
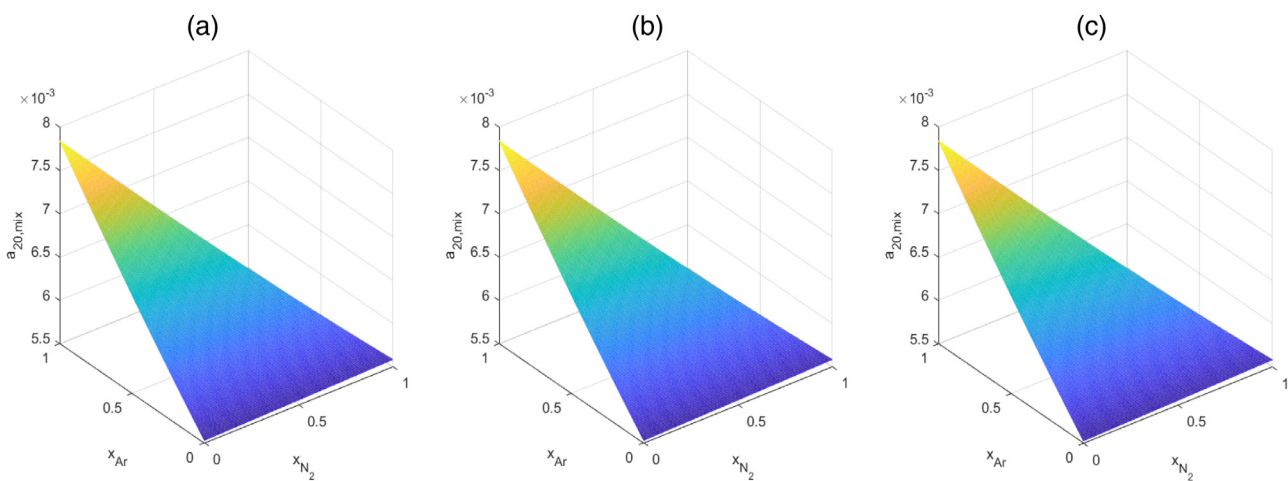
$$\text{variation} = 1 - \frac{Y(T)}{Y(60 \text{ K})} \quad (\text{B.1})$$

Where Y is the generic mixing coefficient.

As it can be observed, the temperature strongly influences the mixing coefficients. The only exceptions are $a_{1\text{mix}}$, $a_{2\text{mix}}$ and $a_{20\text{mix}}$ coefficients which are insensible to the temperature effects. From **Table B.1** it emerges that temperature-dependent coefficients change the order of magnitude (generally, a decreasing trend is registered with temperature) and even the sign. For instance, coefficients E, F, and G present opposite signs for maximum and minimum values meaning that also the phase composition covers a key role in determining the sign of mixing coefficient and in Omega function in Eq.7. The large variability for the mixing coefficient is undesired since it may cause potential numerical instabilities in the solution of the bubble and dew problems.

Table B.1
Maximum and minimum value of mixing coefficients at different temperatures.

	60 K max	min	90 K max	min	120 K max	min
$a_{1\text{mix}}$	0.377	0.317	0.377	0.317	0.377	0.317
$a_{2\text{mix}}$	144	118	144	118	144	118
$a_{20\text{mix}}$	$7.85 \cdot 10^{-3}$	$5.53 \cdot 10^{-3}$	$7.85 \cdot 10^{-3}$	$5.53 \cdot 10^{-3}$	$7.85 \cdot 10^{-3}$	$5.53 \cdot 10^{-3}$
B	2.559	1.401	0.8015	0.6835	0.3275	0.3203
C	0.1352	0.0782	0.06793	0.03520	0.0426	0.0211
D	$-1.590 \cdot 10^{-3}$	$-7.121 \cdot 10^{-3}$	$-7.642 \cdot 10^{-3}$	$-4.342 \cdot 10^{-3}$	$-3.513 \cdot 10^{-4}$	$-2.952 \cdot 10^{-3}$
E	$2.586 \cdot 10^{-4}$	$-2.945 \cdot 10^{-6}$	$1.651 \cdot 10^{-4}$	$-2.980 \cdot 10^{-7}$	$1.183 \cdot 10^{-4}$	$1.025 \cdot 10^{-6}$
F	$2.904 \cdot 10^{-6}$	$-1.906 \cdot 10^{-6}$	$1.936 \cdot 10^{-6}$	$-1.271 \cdot 10^{-6}$	$1.452 \cdot 10^{-6}$	$-9.531 \cdot 10^{-7}$
G	0.06264	-0.8088	0.02292	-0.07777	5.729 $\cdot 10^{-3}$	-0.0162
H	$6.620 \cdot 10^{-3}$	$1.770 \cdot 10^{-3}$	$9.593 \cdot 10^{-4}$	$6.505 \cdot 10^{-4}$	$2.868 \cdot 10^{-4}$	$2.083 \cdot 10^{-4}$

**Fig. B.1.** sensitivity analysis on coefficient $a_{1,\text{mix}}$.**Fig. B.2.** sensitivity analysis on coefficient $a_{2,\text{mix}}$.**Fig. B.3.** sensitivity analysis on coefficient $a_{20,\text{mix}}$.

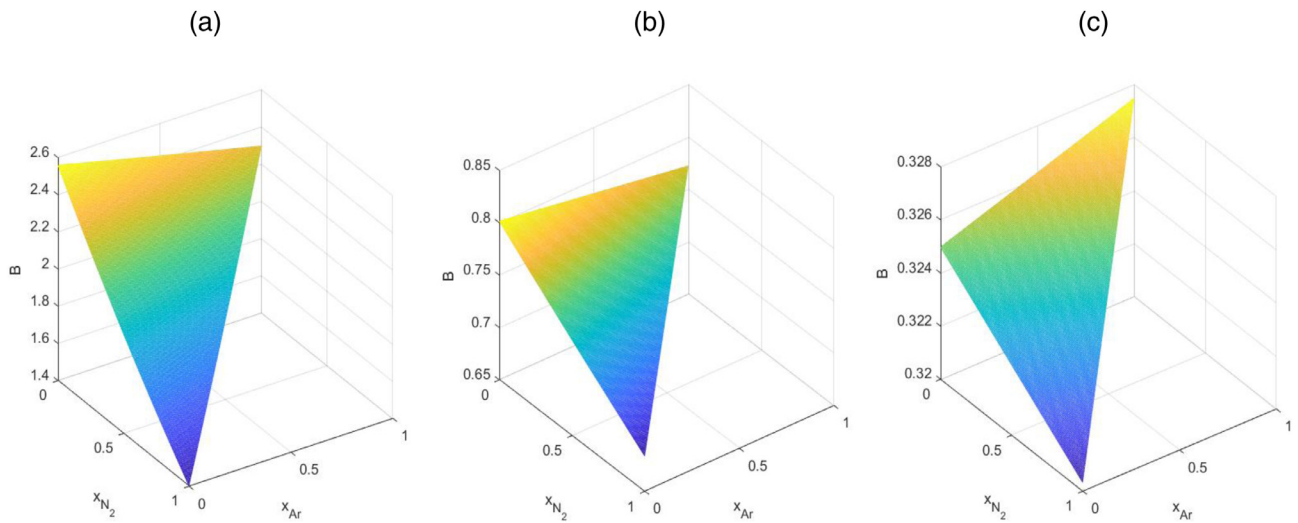


Fig. B.4. sensitivity analysis on coefficient B.

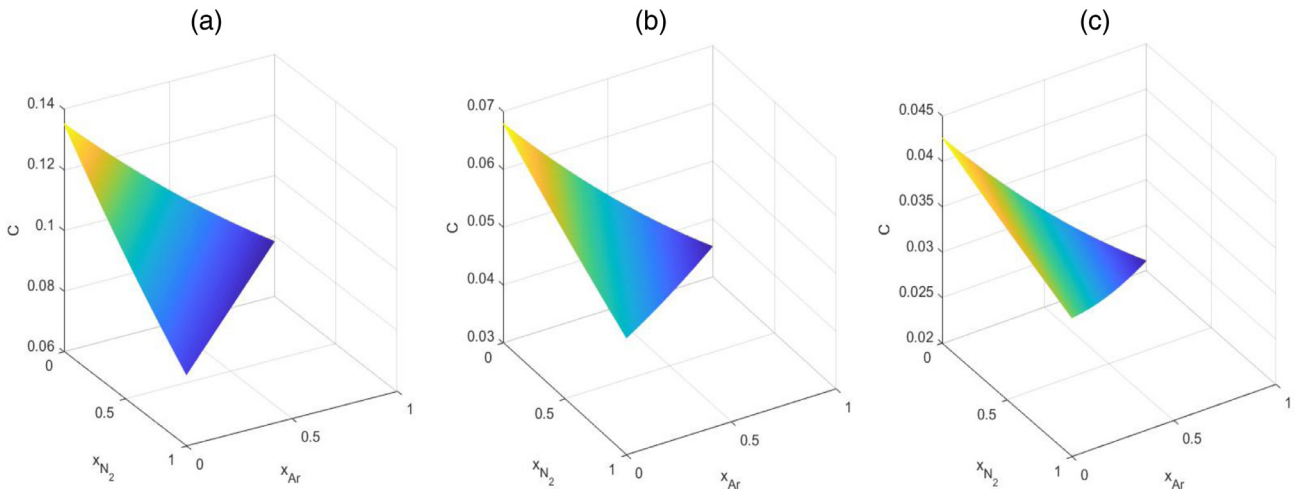


Fig. B.5. sensitivity analysis on coefficient C.

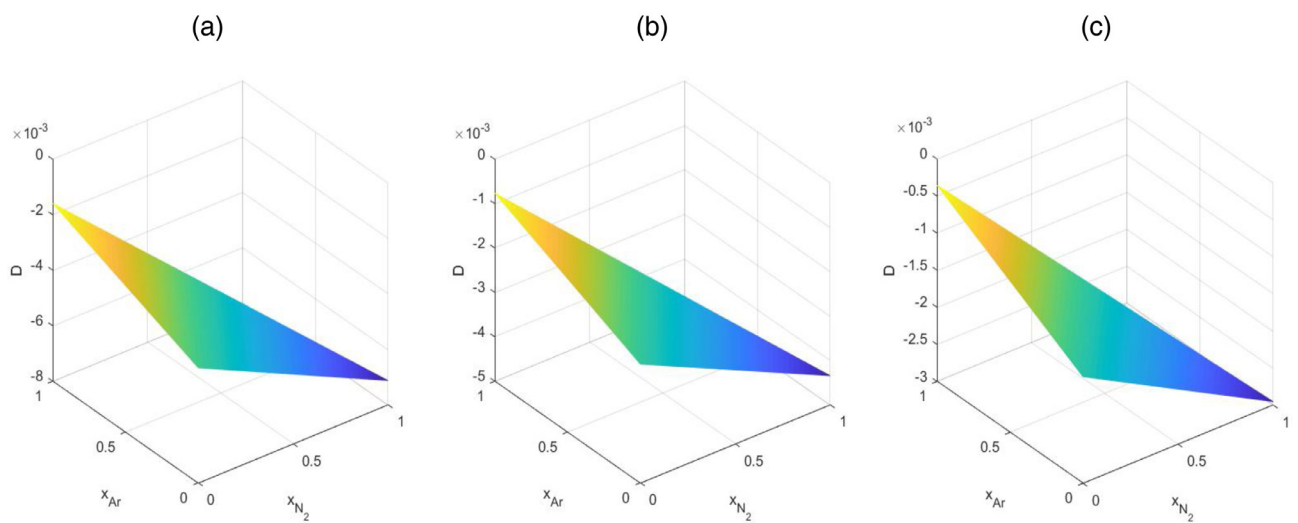
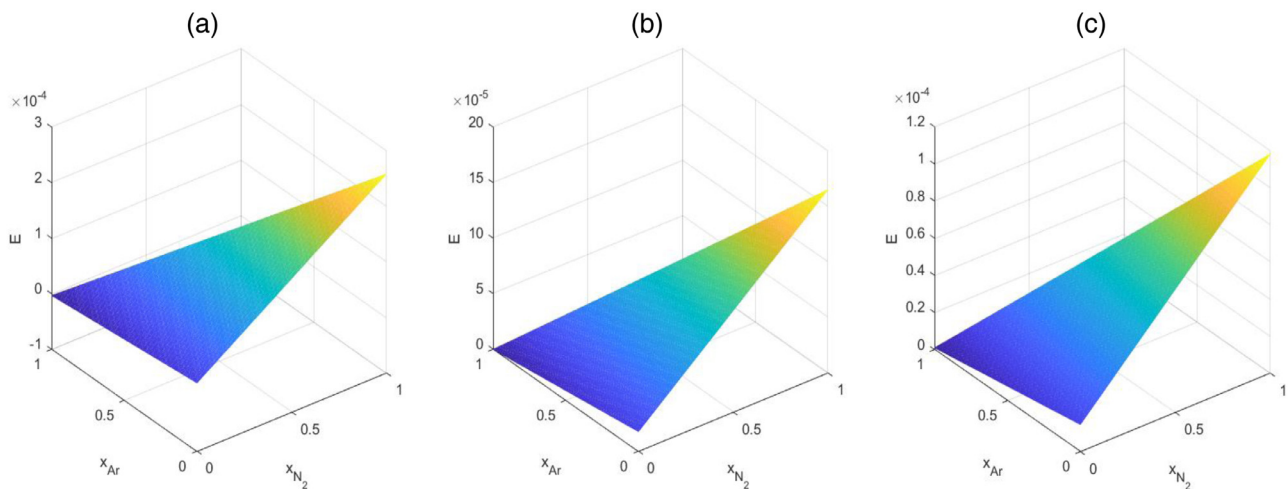
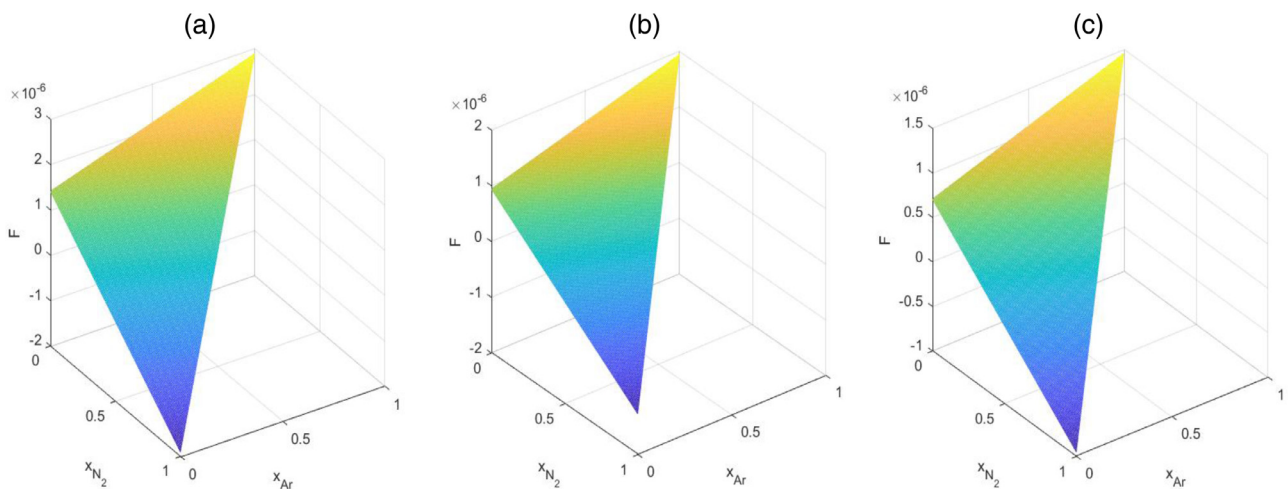
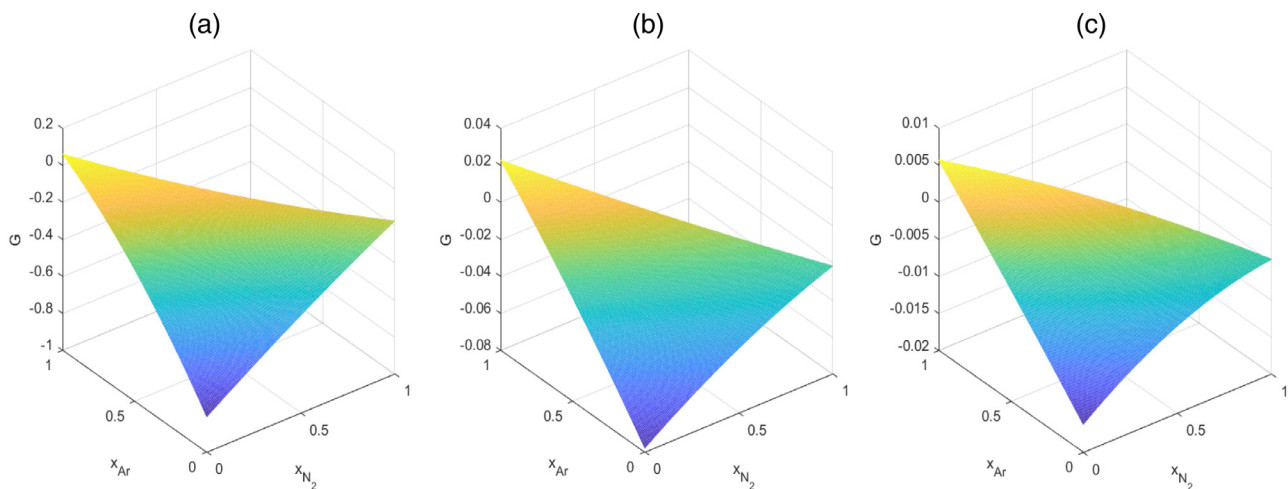


Fig. B.6. sensitivity analysis on coefficient D.

**Fig. B.7.** sensitivity analysis on coefficient E .**Fig. B.8.** sensitivity analysis on coefficient F .**Fig. B.9.** sensitivity analysis on coefficient G .

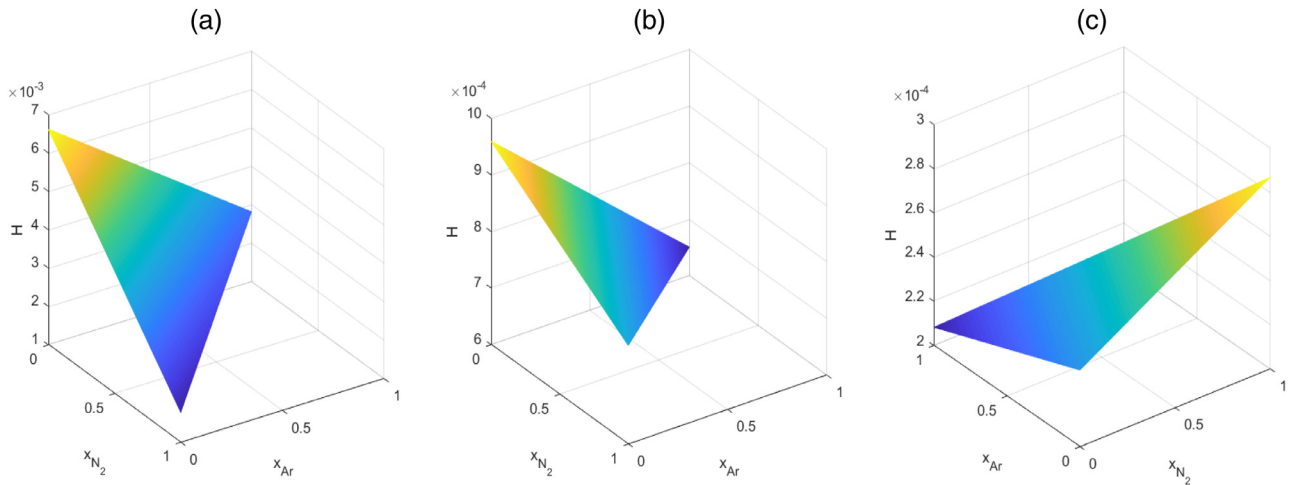


Fig. B.10. sensitivity analysis on coefficient H.

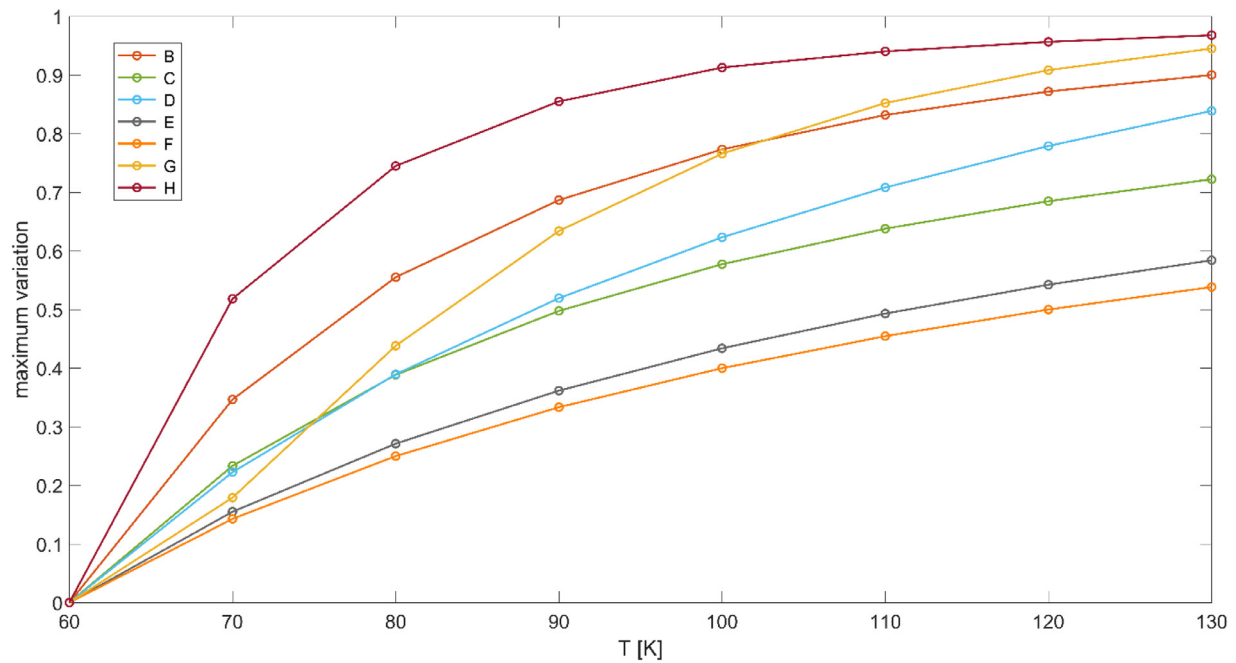


Fig. B11. Percentage variation of maximum values as a function of temperature in cryogenic conditions.

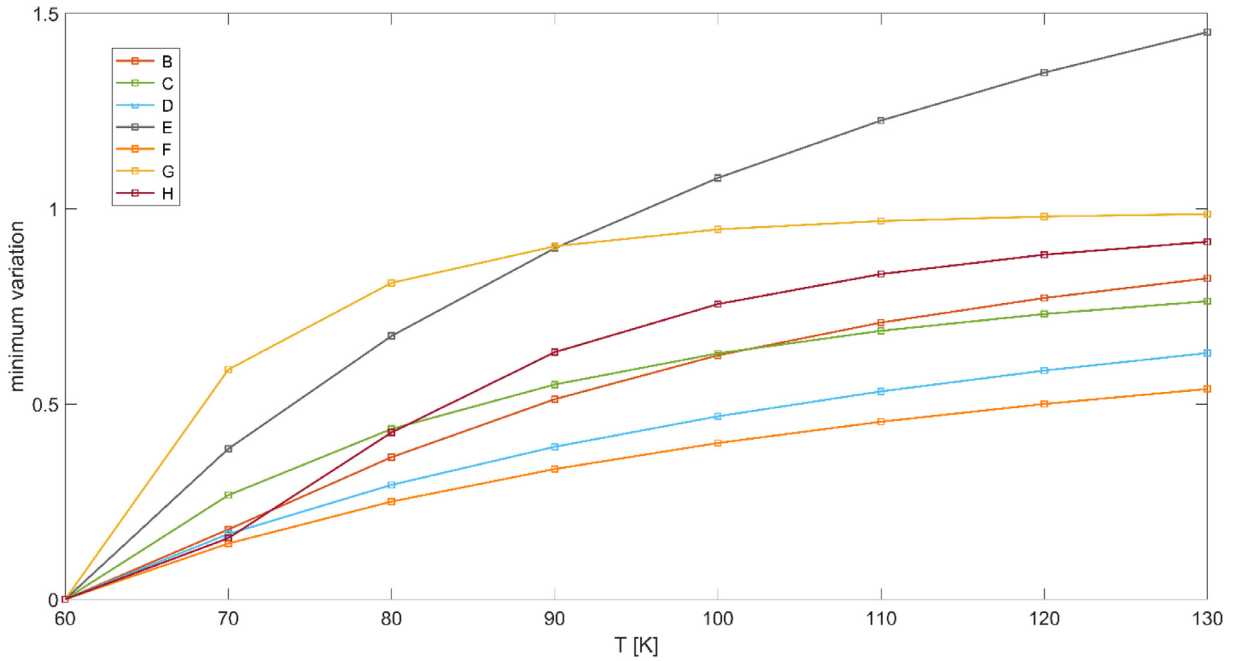


Fig. B12. Percentage variation of minimum values as a function of temperature in cryogenic condition.

Appendix C. – Function steepness

According to Bender NCEoS, predicted pressure is defined as

$$P_{\text{EOS}}(T, d_m, z) = d_m T \left[R + \left(a_1 - \frac{a_2}{T} - B \right) d_m + Cd_m^2 + Dd_m^3 + Ed_m^4 + Fd_m^5 + (G + Hd_m^2)d_m^2 \cdot \exp(-a_{20}d_m^2) \right] \quad (1)$$

In this case, it is of interest to evaluate the displacement between real and predicted pressure ($P_{\text{EOS}} - P$) for density variations ($\pm 1\%$)

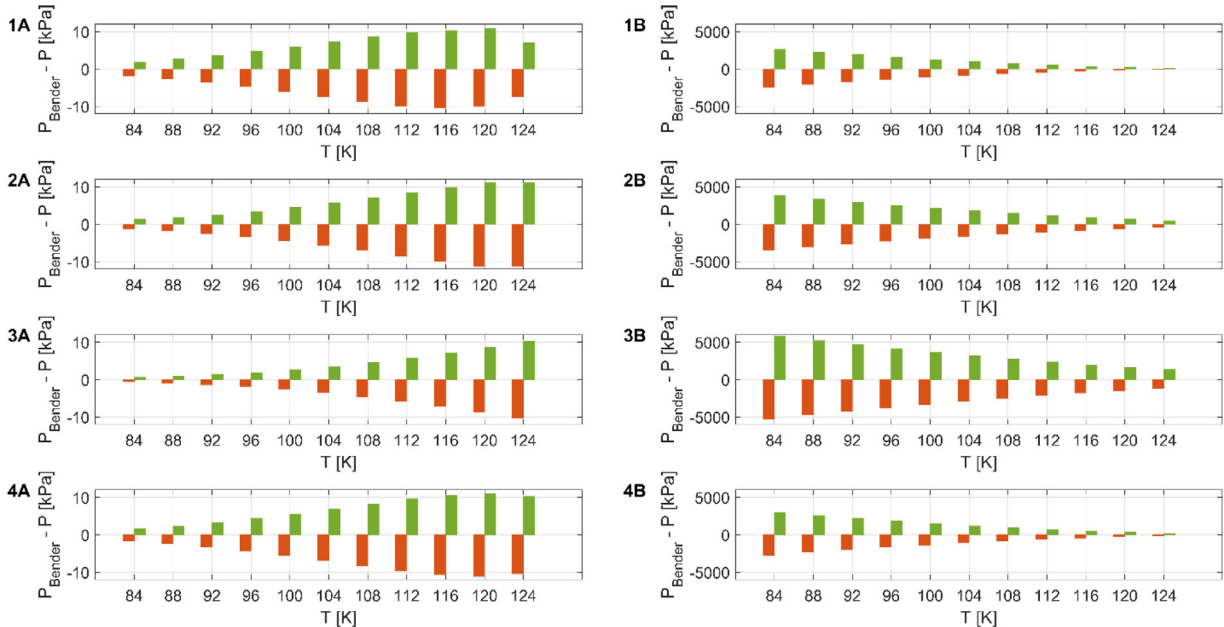


Fig. C1. Error in pressure for positive (green bar) and negative (red bar) density deviations for different N_2 - O_2 binary mixtures: (1) $z_{N_2} = 0.95$, (2) equimolar, (3) $z_{N_2} = 0.05$ and (4) dry air.

around the real root. Exploiting results provided in Bender's work appendix tables, it is possible to

1. assign temperature, pressure, and phases composition at the boiling point,
2. evaluate the corresponding predicted phase molar density,
3. impose variations to the molar density and evaluate the displacement.

Results are indexes of the function steepness and they allow to numerically calculate the derivative of the function Eq. (C1) in the

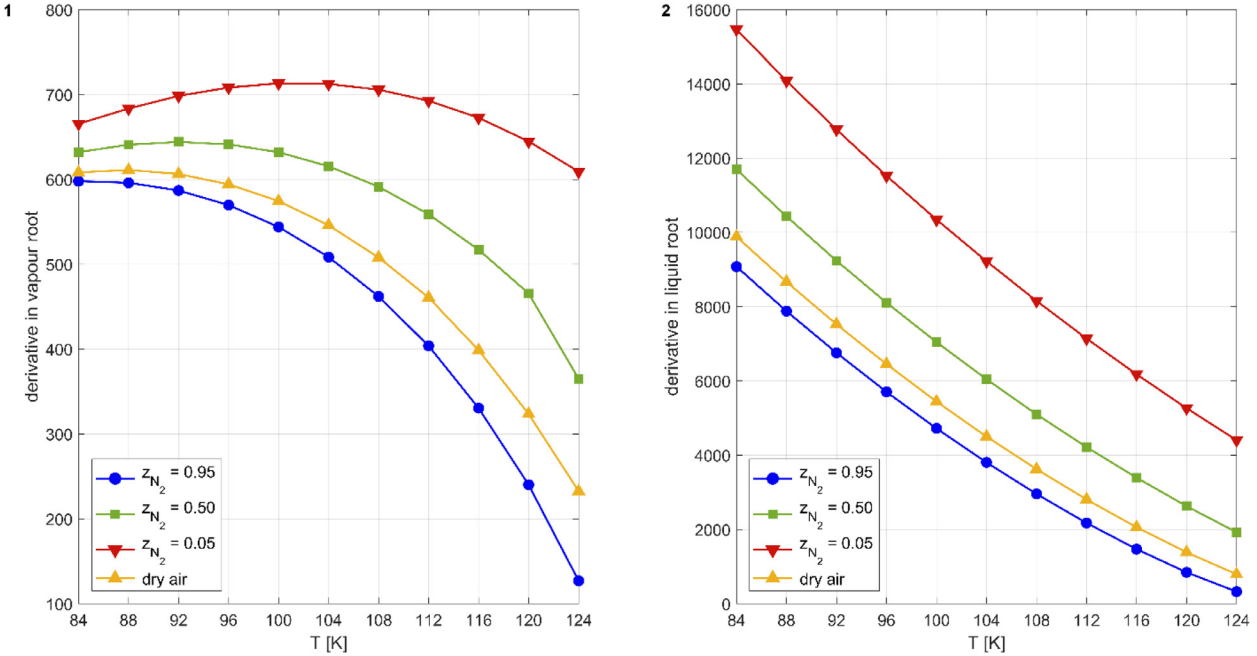


Fig. C2. Derivative in vapour root (A) and liquid (B) for different N_2 - O_2 binary mixtures: (blue) $z_{N_2} = 0.95$, (grey) equimolar, (red) $z_{N_2} = 0.05$ and (yellow) dry air.

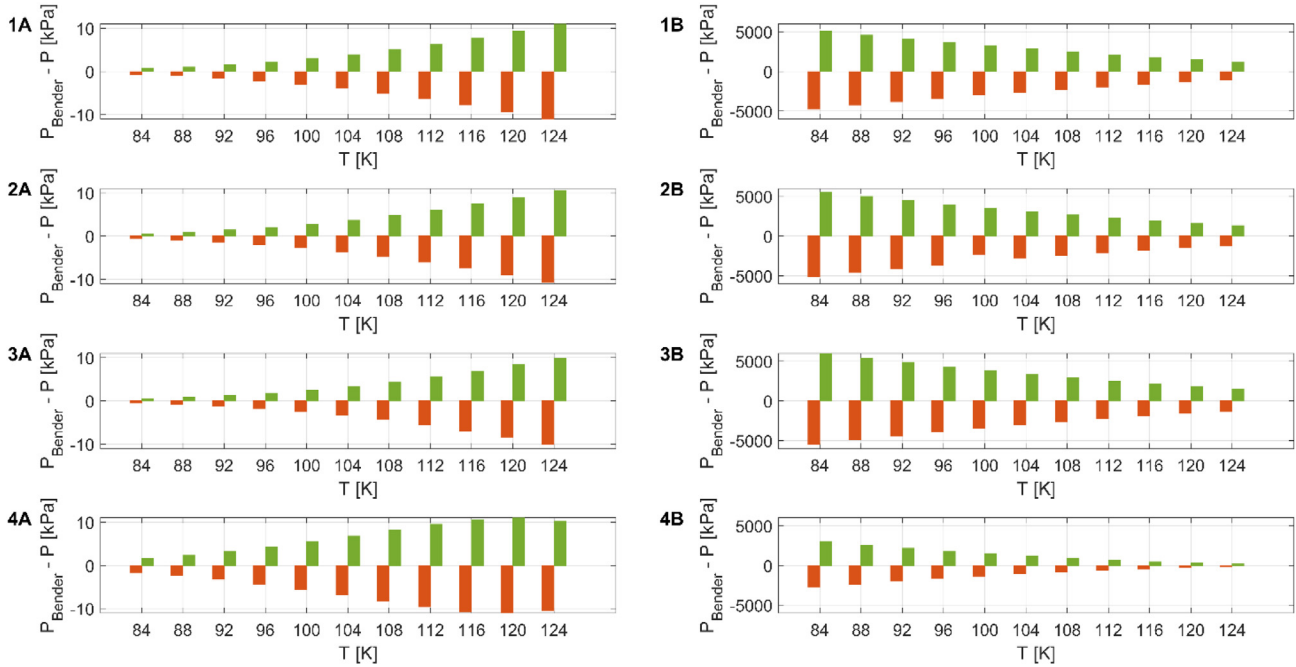


Fig. C3. Error in pressure for positive (green bar) and negative (red bar) density deviations for different Ar - O_2 binary mixtures: (1) $z_{Ar} = 0.90$, (2) equimolar, (3) $z_{Ar} = 0.10$ and (4) dry air.

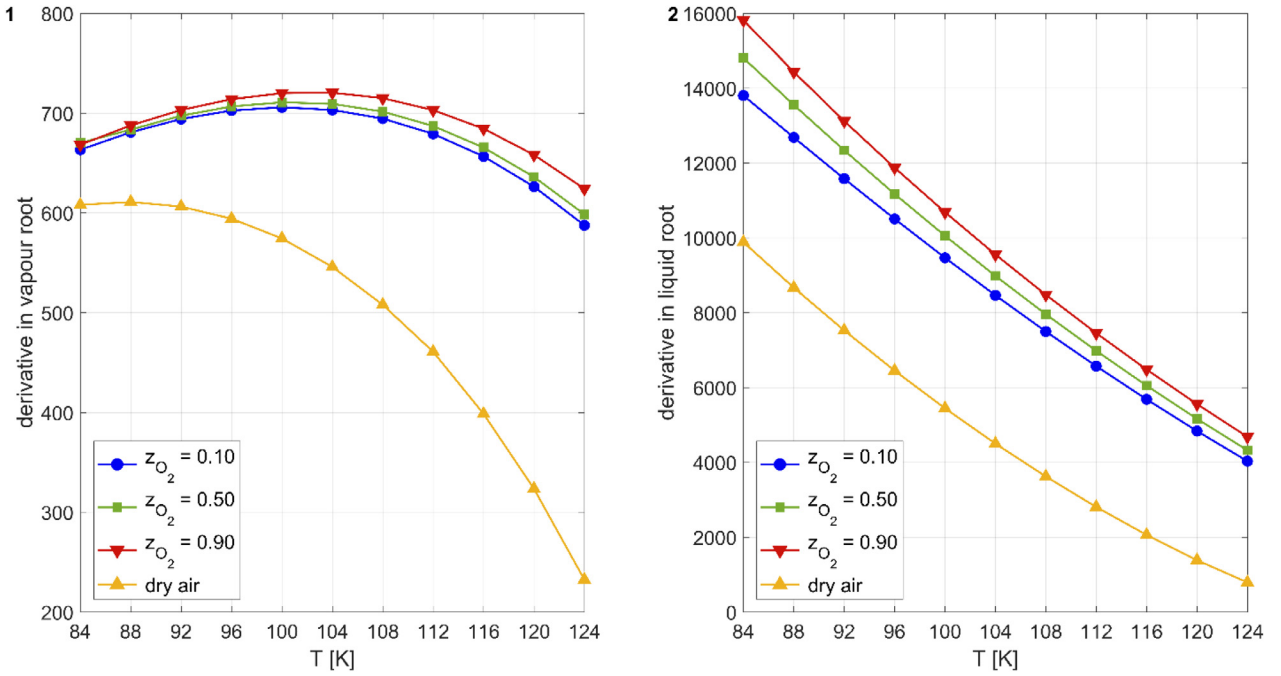


Fig. C4. Derivative in vapour root (A) and liquid (B) for different Ar-O₂ binary mixtures: (green) $z_{Ar} = 0.90$, (grey) equimolar, (red) $z_{Ar} = 0.10$ and (yellow) dry air.

phase root point. Analysis has been done for temperature range and phase composition of interest in ASUs.

Appendix D. – Omega Function general shape

Figures D.1-D.4 show a general shape of the Omega term independently from the phase composition. As in the steepness

analysis, a large amount of oxygen in the mixtures is reflected in larger increments of the function itself close to the zero-level curve (orange line).

$$\Omega(T, d_m, z) = R + \left(a_1 - \frac{a_2}{T} - B \right) d_m + C d_m^2 + D d_m^3 + E d_m^4 + F d_m^5 + (G + H d_m^2) d_m^2 \cdot \exp(-a_{20} d_m^2) \quad (7)$$

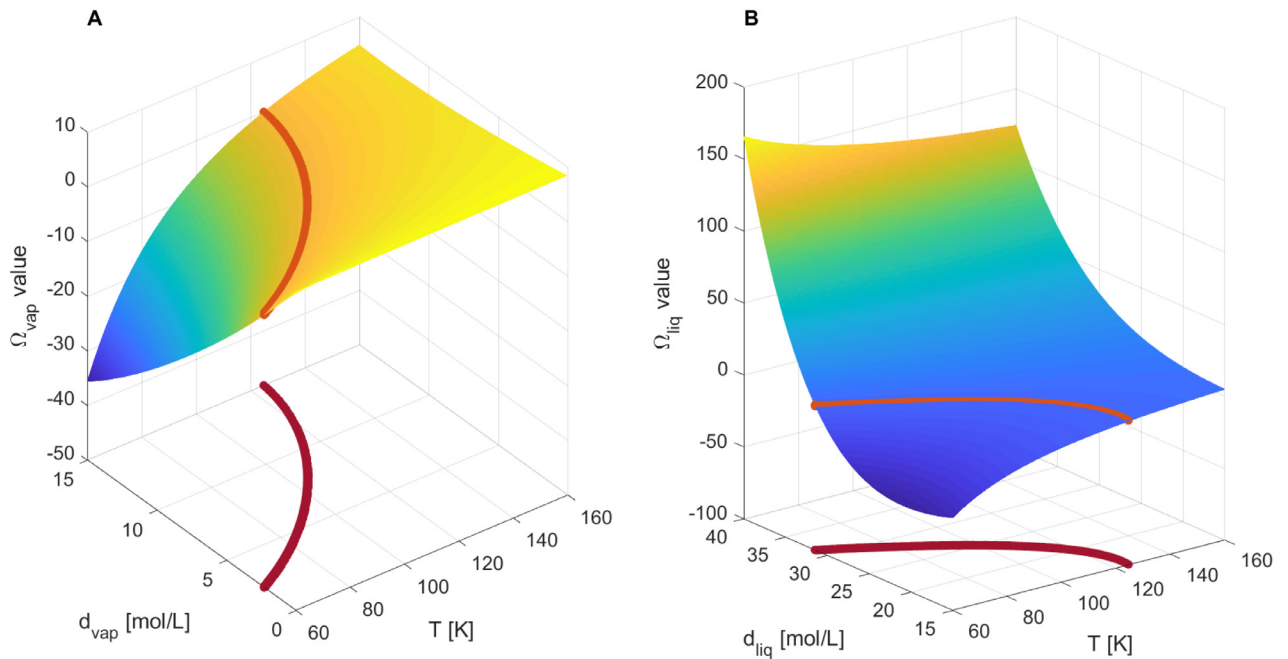


Fig. D1. Pure N₂ Omega function for vapour (A) and liquid (B) phase.

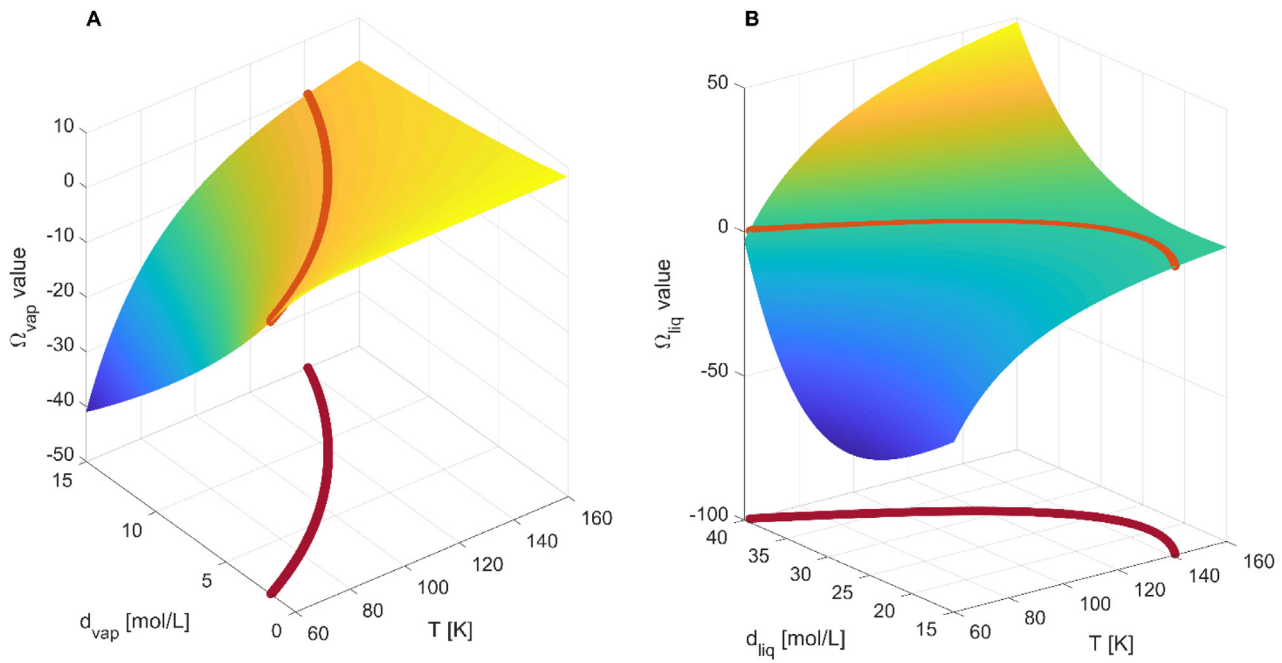


Fig. D2. Pure O₂ Omega function for vapour (A) and liquid (B) phase.

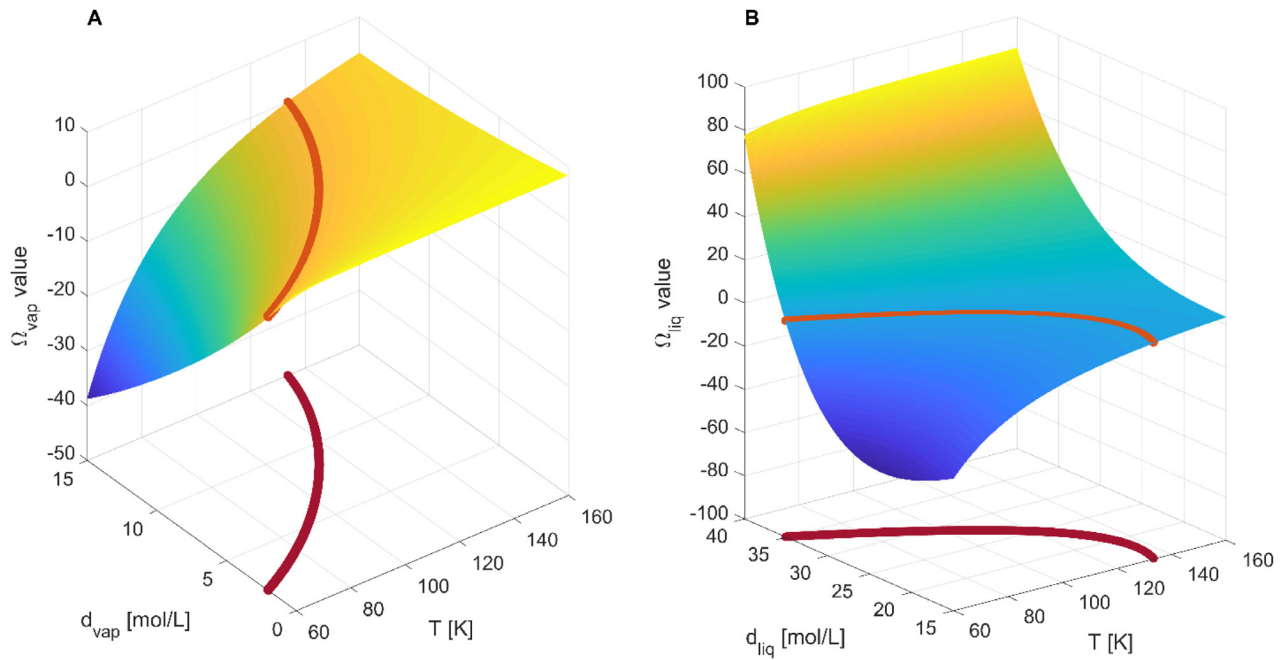


Fig. D3. Equimolar N₂-O₂ Omega function for vapour (A) and liquid (B) phase.

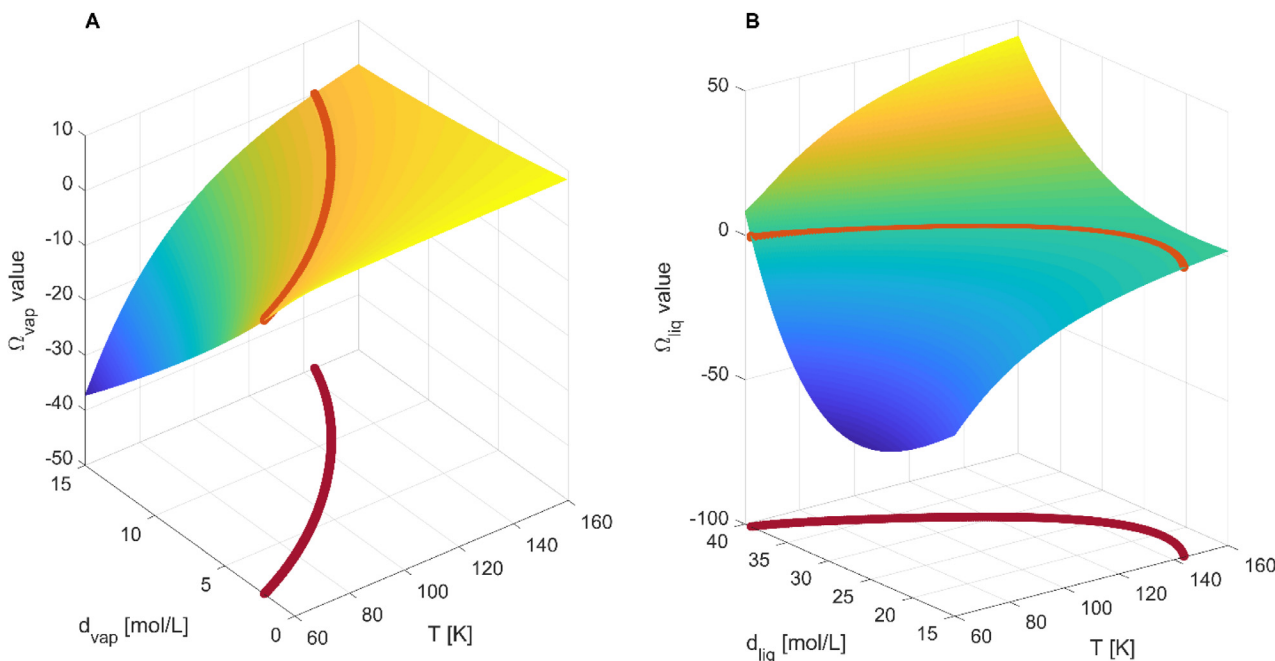


Fig. D4. Equimolar Ar-O₂ Omega function for vapour (A) and liquid (B) phase.

References

- [1] R. Agrawal, R.M. Thorogood, Production of medium pressure nitrogen by cryogenic air separation, *Gas Sep. Purif.* 5 (1991) 203–209, doi: [10.1016/0950-4214\(91\)80025-Z](https://doi.org/10.1016/0950-4214(91)80025-Z).
- [2] R. Agrawal, T.F. Yee, Heat pumps for thermally linked distillation columns: an exercise for argon production from air, *Ind. Eng. Chem. Res.* 33 (1994) 2717–2730, doi: [10.1021/ie00035a023](https://doi.org/10.1021/ie00035a023).
- [3] A. Bassani, G. Bozzano, C. Pirola, C. Frau, A. Pettinai, E. Maggio, E. Ranzi, F. Manenti, Sulfur rich coal gasification and low impact methanol production, *J. Sustain. Devel. Energy, Water Environ. Syst.* 6 (2018) 210–226, doi: [10.13044/j.sdwes.d5.0188](https://doi.org/10.13044/j.sdwes.d5.0188).
- [4] E. Bender, Equations of state for ethylene and propylene, *Cryogenics* 15 (11) (1975) 667–673 15https://doi.org/, doi: [10.1016/0011-2275\(75\)90100-9](https://doi.org/10.1016/0011-2275(75)90100-9).
- [5] E. Bender, *The Calculation of Phase Equilibria from a Thermal Equation of State Applied to the Pure Fluids Argon, Nitrogen, Oxygen and their Mixtures*, C. F. Muller-Verlag, 1973.
- [6] E. Bender, An equation of state for predicting vapour-liquid equilibria of the system N2ArO2, *Cryogenics* 13 (1) (1973) 11–18 13https://doi.org/, doi: [10.1016/0011-2275\(73\)90258-0](https://doi.org/10.1016/0011-2275(73)90258-0).
- [7] E. Bender, Die Berechnung der Verdampfungsgleichgewichte von Mehrstoffsystemen bei hohen Drücken, *Chem. Ing. Tech.* 44 (1972) 576–582, doi: [10.1002/cite.330440816](https://doi.org/10.1002/cite.330440816).
- [8] F. Bisotti, A. di Pretoro, A. Dell'Angelo, D. Previtali, A.F. Amaral, E.M. Andoglu, F. Manenti, Smart implementation of bender equation of state, *Chem. Eng. Trans.* 74 (2019) 715–720, doi: [10.3303/CET1974120](https://doi.org/10.3303/CET1974120).
- [9] T. Bräthen, L.E. Øi, J. Hovland, Simulation of dew points in raw biogas using PR and SRK equations of state, in: Proceedings of The 60th SIMS Conference on Simulation and Modelling SIMS 2019, 170, Västerås, Sweden, 2020, pp. 112–117 August 12-16https://doi.org/, doi: [10.3384/ecp20170112](https://doi.org/10.3384/ecp20170112).
- [10] K. Buhner, G. Maurer, E. Bender, Pressure-enthalpy diagrams for methane, ethane, propane, ethylene and propylene, *Cryogenics* 21 (3) (1981) 157–164 100.
- [11] G. Buzzi-Ferraris, New trends in building numerical programs, *Comput. Chem. Eng.* 35 (2011) 1215–1225, doi: [10.1016/j.compchemeng.2010.07.004](https://doi.org/10.1016/j.compchemeng.2010.07.004).
- [12] G. Buzzi-Ferraris, F. Manenti, Nonlinear Systems and Optimization for the Chemical Engineer: Solving Numerical Problems, Wiley-VCH, 2013, doi: [10.1002/9783527667147](https://doi.org/10.1002/9783527667147).
- [13] C.C. Chen, P.M. Mathias, Applied thermodynamics for process modeling, *AIChE J.* 48 (2002) 194–200, doi: [10.1002/aic.690480202](https://doi.org/10.1002/aic.690480202).
- [14] G.F. Chou, J.M. Prausnitz, A phenomenological correction to an equation of state for the critical region, *AIChE J.* 35 (1989) 1487–1496, doi: [10.1002/aic.690350909](https://doi.org/10.1002/aic.690350909).
- [15] I. Cibulká, J. Kováčiková, L. Hnědkovský, J.P. Novák, A simple method for evaluation of parameters of the Bender equation of state from experimental data, *Fluid Phase Equilibr.* 180 (2001) 27–40, doi: [10.1016/S0378-3812\(00\)00494-5](https://doi.org/10.1016/S0378-3812(00)00494-5).
- [16] M. Corbetta, I.E. Grossmann, F. Manenti, Process simulator-based optimization of biorefinery downstream processes under the Generalized Disjunctive Programming framework, *Comput. Chem. Eng.* 88 (2016) 73–85, doi: [10.1016/j.compchemeng.2016.02.009](https://doi.org/10.1016/j.compchemeng.2016.02.009).
- [17] M. Corbetta, I.E. Grossmann, F. Manenti, M. Bernardi, A. Frattini, Systematic Design of the Green Ethylene Glycol Downstream Process under the Generalized Disjunctive Programming Framework, Computer Aided Chemical Engineering, Elsevier Masson SAS, 2016, doi: [10.1016/B978-0-444-63428-3.50389-1](https://doi.org/10.1016/B978-0-444-63428-3.50389-1).
- [18] M. Corbetta, C. Pirola, F. Galli, F. Manenti, Robust optimization of the heteroextractive distillation column for the purification of water/acetic acid mixtures using p-xylene as entrainer, *Comput. Chem. Eng.* 95 (2016) 161–169, doi: [10.1016/j.compchemeng.2016.09.015](https://doi.org/10.1016/j.compchemeng.2016.09.015).
- [19] N.A. Darwish, R.A. Al-Mehaideb, A.M. Braek, R. Hughes, Computer simulation of BTEX emission in natural gas dehydration using PR and RKs equations of state with different predictive mixing rules, *Environ. Model. Softw.* 19 (2004) 957–965, doi: [10.1016/j.envsoft.2003.10.008](https://doi.org/10.1016/j.envsoft.2003.10.008).
- [20] G. De Guido, S. Langé, S. Moioli, L.A. Pellegrini, Thermodynamic method for the prediction of solid CO₂ formation from multicomponent mixtures, *Process Saf. Environ. Prot.* 92 (2014) 70–79, doi: [10.1016/j.psep.2013.08.001](https://doi.org/10.1016/j.psep.2013.08.001).
- [21] Y. Dong, R. Zhu, Y. Guo, Z. Lei, A united chemical thermodynamic model: COSMO-UNIFAC, *Ind. Eng. Chem. Res.* 57 (2018) 15954–15958, doi: [10.1021/acs.iecr.8b04870](https://doi.org/10.1021/acs.iecr.8b04870).
- [22] I.M. Elshayal, B.C.Y. Lu, Vapor-liquid equilibrium data for nitrogen-argon-oxygen mixtures evaluation and correlation, *J. Chem. Eng. Data* 16 (1971) 31–37, doi: [10.1016/j.ee60048a012](https://doi.org/10.1016/j.ee60048a012).
- [23] D.M. Espie, S. Macchietto, Nonlinear transformations for parameter estimation, *Ind. Eng. Chem. Res.* 27 (1988) 2175–2179, doi: [10.1021/je00083a037](https://doi.org/10.1021/je00083a037).
- [24] EUROPEAN INDUSTRIAL GASES ASSOCIATION AISBL, *Safe Practices Guide for Cryogenic Air Separation Plants Safe Practices Guide for Cryogenic*, 2005.
- [25] G., L.A. Forero, J., J.A. Velásquez, The Patel-Teja and the Peng-Robinson EoSs performance when Soave alpha function is replaced by an exponential function, *Fluid Phase Equilibr.* 332 (2012) 55–76, doi: [10.1016/j.fluid.2012.05.026](https://doi.org/10.1016/j.fluid.2012.05.026).
- [26] Q. Fu, L. Zhu, X. Chen, Complete equation-oriented approach for process analysis and optimization of a cryogenic air separation unit, *Ind. Eng. Chem. Res.* 54 (2015) 12096–12107, doi: [10.1021/acs.iecr.5b02768](https://doi.org/10.1021/acs.iecr.5b02768).
- [27] R. Gani, J. Baldyga, B. Biscans, E. Brunazzi, J.C. Charpentier, E. Drioli, H. Feise, A. Furlong, K.M. Van Geem, J.C. de Hemptinne, A.J.B. ten Kate, G.M. Kontogeorgis, F. Manenti, G.B. Marin, S.S. Mansouri, P.M. Piccione, A. Povoa, M.A. Rodrigo, B. Sarup, E. Sørensen, I.A. Udagama, J.M. Woodley, A multi-layered view of chemical and biochemical engineering, *Chem. Eng. Res. Des.* 155 (2020) 133–145, doi: [10.1016/j.cherd.2020.01.008](https://doi.org/10.1016/j.cherd.2020.01.008).
- [28] J. Gernert, R. Span, EOS-CG: a Helmholtz energy mixture model for humid gases and CCS mixtures, *J. Chem. Thermodyn.* 93 (2016) 274–293, doi: [10.1016/j.jct.2015.05.015](https://doi.org/10.1016/j.jct.2015.05.015).
- [29] J. Ghazouani, O. Chouaib, A. Bellagi, Evaluation of the parameters of the Bender equation of state for low acentric factor fluids and carbon dioxide, *Thermochim. Acta* 432 (2005) 10–19, doi: [10.1016/j.tca.2004.11.008](https://doi.org/10.1016/j.tca.2004.11.008).
- [30] R. Gosset, G. Heyen, B. Kalitventzoff, An efficient algorithm to solve cubic equation of state, *Fluid Phase Equilibr.* 25 (1986) 51–64.
- [31] E. Hendriks, G.M. Kontogeorgis, R. Dohrn, J.C. De Hemptinne, I.G. Economou, L.F. Žilnik, V. Vesovic, Industrial requirements for thermodynamics and transport properties, *Ind. Eng. Chem. Res.* 49 (2010) 11131–11141, doi: [10.1021/ie101231b](https://doi.org/10.1021/ie101231b).
- [32] M. Ibrahim, G. Skaugeen, I.S. Ertesvåg, An extended corresponding states equation of state (EoS) for CCS industry, *Chem. Eng. Sci.* 137 (2015) 572–582, doi: [10.1016/j.ces.2015.06.013](https://doi.org/10.1016/j.ces.2015.06.013).

- [33] S.L. Jenkins, A.K. Majumdar, R.C. Hendricks, Investigation of two and Three Parameter Equations of State for Cryogenic Fluids BT - Advances in Cryogenic Engineering: Part A & B, Springer US, Boston, MA, 1990, pp. 1487–1494 Fast, R.W. <https://doi.org/>, doi: [10.1007/978-1-4613-0639-9_176](https://doi.org/10.1007/978-1-4613-0639-9_176).
- [34] R.S. Kamath, L.T. Biegler, I.E. Grossmann, Modeling multistream heat exchangers with and without phase changes for simultaneous optimization and heat integration, *AIChE J.* 59 (2012) 215–228, doi: [10.1002/aic](https://doi.org/10.1002/aic).
- [35] R.S. Kamath, I.E. Grossmann, L.T. Biegler, S.E. Zitney, *Optimal Integrated Design of Air Separation Unit and Gas Turbine Block for IGCC Systems*, 2009 United States.
- [36] C.J. Kedge, M.A. Trebble, An empirical near-critical correction for cubic and non-cubic equations of state, *Fluid Phase Equilib.* 194–197 (2002) 401–409, doi: [10.1016/S0378-3812\(01\)00773-7](https://doi.org/10.1016/S0378-3812(01)00773-7).
- [37] H. Kwang Bae, K. Nagahama, M. Hirata, Evaluation and correlation of vapor-liquid equilibria in the ternary system nitrogen-argon-oxygen, *Fluid Phase Equilib.* 4 (1980) 45–60.
- [38] S. Lasala, P. Chiesa, R. Privat, J.N. Jaubert, Sizing and operating units for the purification and compression of CO₂-based streams: the impact of thermodynamic model accuracy, *J. Supercrit. Fluids* 140 (2018) 336–347, doi: [10.1016/j.supflu.2018.04.010](https://doi.org/10.1016/j.supflu.2018.04.010).
- [39] Silvia Lasala, P. Chiesa, R. Privat, J.N. Jaubert, Modeling the thermodynamics of fluids treated by CO₂ capture processes with peng-robinson + residual helmholtz energy-based mixing rules, *Ind. Eng. Chem. Res.* 56 (2017) 2259–2276, doi: [10.1021/acs.iecr.6b04190](https://doi.org/10.1021/acs.iecr.6b04190).
- [40] S. Lasala, R. Privat, J.-N. Jaubert, The Impact of Thermodynamic Model Accuracy on Sizing and Operating CCS Purification and Compression Units, *Cutting Edge for Carbon Capture Utilization and Storage*, 2017, doi: [10.1002/9781119363804.ch22](https://doi.org/10.1002/9781119363804.ch22).
- [41] S. Lasala, R. Privat, J.N. Jaubert, P. Arpentier, Modelling the thermodynamics of air-component mixtures (N₂, O₂ and Ar): comparison and performance analysis of available models, *Fluid Phase Equilib.* 458 (2018) 278–287, doi: [10.1016/j.fluid.2017.10.033](https://doi.org/10.1016/j.fluid.2017.10.033).
- [42] R.E. Latimer, Vapor-liquid equilibria of nitrogen-argon-oxygen mixtures, *AIChE J.* 3 (1957) 75–82, doi: [10.1002/aic.690030114](https://doi.org/10.1002/aic.690030114).
- [43] Y. Le Guennec, S. Lasala, R. Privat, J.N. Jaubert, A consistency test for α -functions of cubic equations of state, *Fluid Phase Equilib.* 427 (2016) 513–538 <https://doi.org/>, doi: [10.1016/j.fluid.2016.07.026](https://doi.org/10.1016/j.fluid.2016.07.026).
- [44] T. Ledent, G. Heyen, Dynamic approximation of thermodynamic properties by means of local models, *Comput. Chem. Eng.* 18 (1994) S87–S91, doi: [10.1016/0098-1354\(94\)80015-4](https://doi.org/10.1016/0098-1354(94)80015-4).
- [45] M.E. Leesley, G. Heyen, The dynamic approximation method of handling vapor-liquid equilibrium data in computer calculations for chemical processes, *Comput. Chem. Eng.* 1 (1977) 103–108, doi: [10.1016/0098-1354\(77\)80015-X](https://doi.org/10.1016/0098-1354(77)80015-X).
- [46] Z. Lei, B. Chen, C. Li, H. Liu, Predictive molecular thermodynamic models for liquid solvents, solid salts, polymers, and ionic liquids, *Chem. Rev.* 108 (2008) 1419–1455, doi: [10.1021/cr068441+](https://doi.org/10.1021/cr068441+).
- [47] E.W. Lemmon, R.T. Jacobsen, A new functional form and new fitting techniques for equations of state with application to pentafluoroethane (HFC-125), *J. Phys. Chem. Ref. Data* 34 (2005) 69–108, doi: [10.1063/1.1797813](https://doi.org/10.1063/1.1797813).
- [48] E.W. Lemmon, R.T. Jacobsen, S.G. Penoncello, D.G. Friend, Thermodynamic properties of air and mixtures of nitrogen, argon, and oxygen from 60 to 2000 K at pressures to 2000 MPa, *J. Phys. Chem. Ref. Data* (2000), doi: [10.1063/1.1285884](https://doi.org/10.1063/1.1285884).
- [49] L. Li, J. Zhao, H. Li, L. Zhang, S. Fan, Q. Li, W. Pang, X. Lü, L. Zheng, N. Wei, A novel fitted thermodynamic model for the capture of CO₂ from flue gas by the hydrate method, *Natural Gas Industry B* 6 (2019) 603–609, doi: [10.1016/j.ngib.2019.04.006](https://doi.org/10.1016/j.ngib.2019.04.006).
- [50] P. Liu, E.N. Pistikopoulos, A multi-objective optimization approach to polygeneration energy systems design, *AIChE J.* 56 (2009) 1218–1234, doi: [10.1002/aic](https://doi.org/10.1002/aic).
- [51] J.O. Lloret, L.F. Vega, F. Llorell, A consistent and transferable thermodynamic model to accurately describe CO₂ capture with monoethanolamine, *J. CO₂ Utiliz.* 21 (2017) 521–533, doi: [10.1016/j.jcou.2017.08.018](https://doi.org/10.1016/j.jcou.2017.08.018).
- [52] J.S. Lopez-Echeverry, S. Reif-Acherman, E. Araujo-Lopez, Peng-Robinson equation of state: 40 years through cubics, *Fluid Phase Equilib.* 447 (2017) 39–71, doi: [10.1016/j.fluid.2017.05.007](https://doi.org/10.1016/j.fluid.2017.05.007).
- [53] S. Macchietto, G.I. Maduabueke, R. Szczepanski, Efficient implementation of VLE procedures in equation-oriented simulators, *AIChE J.* 34 (1988) 955–963, doi: [10.1002/aic.690340608](https://doi.org/10.1002/aic.690340608).
- [54] J.A. Mandler, D.R. Vinson, N. Chatterjee, Dynamic modelling and control of cryogenic AIR separation plants, *IFAC Proceedings Volumes*, 22, 1989, pp. 267–273, doi: [10.1016/s1474-6670\(17\)53367-4](https://doi.org/10.1016/s1474-6670(17)53367-4).
- [55] F. Manenti, G. Buzzi-Ferraris, A new strategy to improve parameter estimation, *Chem. Eng. Trans.* 17 (2009) 1335–1340.
- [56] F. Manenti, Considerations on nonlinear model predictive control techniques, *Comput. Chem. Eng.* 35 (2011) 2491–2509, doi: [10.1016/j.compchemeng.2011.04.009](https://doi.org/10.1016/j.compchemeng.2011.04.009).
- [57] F. Manenti, I. Dones, G. Buzzi-Ferraris, H.A. Preisig, Efficient numerical solver for partially structured differential and algebraic equation systems, *Ind. Eng. Chem. Res.* 48 (2009) 9979–9984, doi: [10.1021/ie9007908](https://doi.org/10.1021/ie9007908).
- [58] P. Nimmegeers, M. Vallerio, D. Telen, J. Van Impe, F. Logist, Interactive multi-objective dynamic optimization of bioreactors under parametric uncertainty, *Chem. Ing. Tech.* 91 (2019) 349–362, doi: [10.1002/cite.201800082](https://doi.org/10.1002/cite.201800082).
- [59] N. Patel, A. Teja, A three-parameter cubic equation of state for fluids and fluid mixtures4, *Can. J. Chem. Eng.* 37 (1982) 463–473, doi: [10.1002/cjce.5450680319](https://doi.org/10.1002/cjce.5450680319).
- [60] L.A. Pellegrini, G. De Guido, S. Langé, Biogas to liquefied biomethane via cryogenic upgrading technologies, *Renewable Energy* 124 (2018) 75–83, doi: [10.1016/j.renene.2017.08.007](https://doi.org/10.1016/j.renene.2017.08.007).
- [61] L.A. Pellegrini, G. Soave, S. Gamba, S. Langé, Economic analysis of a combined energy-methanol production plant, *Appl. Energy* 88 (2011) 4891–4897 <https://doi.org/>, doi: [10.1016/j.apenergy.2011.06.028](https://doi.org/10.1016/j.apenergy.2011.06.028).
- [62] D.Y. Peng, D.B. Robinson, A new two-constant equation of state, *Ind. Eng. Chem. Fundam.* 15 (1976) 59–64, doi: [10.1021/i160057a011](https://doi.org/10.1021/i160057a011).
- [63] R.H. Perry, D.W. Green, *Perry's Chemical Engineers' Handbook*, 8th Ed., 2013, doi: [10.1017/CBO9781107415324.004](https://doi.org/10.1017/CBO9781107415324.004).
- [64] A. Pfennig, *Thermodynamik der Gemische*, 1st Ed., Springer, Berlin, Heidelberg, 2004 <https://doi.org/>, doi: [10.1007/978-3-642-18923-4](https://doi.org/10.1007/978-3-642-18923-4).
- [65] A. Piña-Martínez, R. Privat, J.N. Jaubert, D.Y. Peng, Updated versions of the generalized Soave α -function suitable for the Redlich-Kwong and Peng-Robinson equations of state, *Fluid Phase Equilib.* 485 (2019) 264–269, doi: [10.1016/j.fluid.2018.12.007](https://doi.org/10.1016/j.fluid.2018.12.007).
- [66] A. Piña-Martínez, R. Privat, S. Lasala, G. Soave, J.N. Jaubert, Search for the optimal expression of the volumetric dependence of the attractive contribution in cubic equations of state, *Fluid Phase Equilib.* 522 (2020), doi: [10.1016/j.fluid.2020.112750](https://doi.org/10.1016/j.fluid.2020.112750).
- [67] C. Pirola, F. Galli, F. Manenti, M. Corbetta, C.L. Bianchi, Simulation and related experimental validation of acetic acid/water distillation using p-xylene as entrainer, *Ind. Eng. Chem. Res.* 53 (2014) 18063–18070, doi: [10.1021/ie502758v](https://doi.org/10.1021/ie502758v).
- [68] B. Platzer, G. Maurer, A generalized equation of state for pure polar and nonpolar fluids, *Fluid Phase Equilib.* 51 (1989) 223–236.
- [69] B. Platzer, G. Maurer, Application of a generalized Bender equation of state to the description of vapour-liquid equilibria in binary systems, *Fluid Phase Equilib.* (1993), doi: [10.1016/0378-3812\(93\)85118-6](https://doi.org/10.1016/0378-3812(93)85118-6).
- [70] A. Polt, G. Maurer, The bender equation of state for describing thermodynamic properties of krypton, neon, fluorine, sulfur dioxide and water over a wide range of state, *Fluid Phase Equilib.* 73 (1992) 27–38, doi: [10.1016/0378-3812\(92\)85037-9](https://doi.org/10.1016/0378-3812(92)85037-9).
- [71] M.V. Rocco, S. Langé, L. Pigoli, E. Colombo, L.A. Pellegrini, Assessing the energy intensity of alternative chemical and cryogenic natural gas purification processes in LNG production, *J. Cleaner Prod.* 208 (2019) 827–840, doi: [10.1016/j.jclepro.2018.10.108](https://doi.org/10.1016/j.jclepro.2018.10.108).
- [72] B. Seliger, R. Hanke-Rauschenbach, F. Hannemann, K. Sundmacher, Modelling and dynamics of an air separation rectification column as part of an IGCC power plant, *Separat. Purific. Technol.* 49 (2006) 136–148, doi: [10.1016/j.seppur.2005.09.007](https://doi.org/10.1016/j.seppur.2005.09.007).
- [73] H. Shuen-Cheng, Vapor-liquid equilibrium calculations for N₂-Ar-O₂ Mixtures with modified BWR equation of state and corrisponding states principle, *Fluid Phase Equilib.* 37 (1987) 153–167.
- [74] U. Sievers, S. Schulz, An equation of state for methane in the form of Bender's equation for temperatures between 91 K and 625 K and pressures up to 500 bar, *Fluid Phase Equilib.* 5 (1980) 35–54, doi: [10.1016/0378-3812\(80\)80042-2](https://doi.org/10.1016/0378-3812(80)80042-2).
- [75] J.M. Smith, H.C. Van Ness, M.M. Abbott, M.T. Swihart, *Introduction To Chemical Engineering Thermodynamics Eighth Edition*, McGraw Hill Educational, 2018.
- [76] G. Soave, Equilibrium constants from a modified Redlich-Kwong equation of state, *Chem. Eng. Sci.* 27 (1972) 1197–1203, doi: [10.1016/0009-2509\(72\)80096-4](https://doi.org/10.1016/0009-2509(72)80096-4).
- [77] G.S. Soave, S. Gamba, L.A. Pellegrini, S. Bonomi, Feed-splitting technique in cryogenic distillation, *Ind. Eng. Chem. Res.* 45 (2006) 5761–5765 <https://doi.org/>, doi: [10.1021/ie051343e](https://doi.org/10.1021/ie051343e).
- [78] R. Stryjek, J.H. Vera, PRSV: an improved peng–Robinson equation of state for pure compounds and mixtures, *Can. J. Chem. Eng.* 64 (1986) 323–333, doi: [10.1002/cjce.5450640224](https://doi.org/10.1002/cjce.5450640224).
- [79] R. Stryjek, J.H. Vera, PRSV – an improved peng–Robinson equation of state with new mixing rules for strongly nonideal mixtures, *Can. J. Chem. Eng.* 64 (1986) 334–340, doi: [10.1002/cjce.5450640225](https://doi.org/10.1002/cjce.5450640225).
- [80] A.S. Teja, A. Singh, Equations of state for ethane, propane and n-butane, *Cryogenics* 17 (11) (1977) 591–596 <https://doi.org/>, doi: [10.1016/0011-2275\(77\)90112-6](https://doi.org/10.1016/0011-2275(77)90112-6).
- [81] S. Tesch, T. Morosuk, G. Tsatsaronis, Comparative Evaluation of Cryogenic Air Separation Units from the Exergetic and Economic Points of View, *Low-temperature Technologies*, 2020, pp. 1–20, doi: [10.5772/intechopen.85765](https://doi.org/10.5772/intechopen.85765).
- [82] M.A. Trebble, A New Four-Parameter Cubic Equation of State For Polar and Non-Polar Fluids. Ph.D Thesis, Calgary, Alberta. 1986, doi: [10.1017/CBO9781107415324.004](https://doi.org/10.1017/CBO9781107415324.004).
- [83] M.A. Trebble, P.R. Bishnoi, Extension of the Trebble-Bishnoi equation of state to fluid mixtures, *Fluid Phase Equilib.* 40 (1988) 1–21, doi: [10.1016/0378-3812\(88\)80020-7](https://doi.org/10.1016/0378-3812(88)80020-7).
- [84] M.A. Trebble, P.R. Bishnoi, Development of a new four-parameter cubic equation of state, *Fluid Phase Equilib.* 35 (1987) 1–18, doi: [10.1016/0378-3812\(87\)80001-8](https://doi.org/10.1016/0378-3812(87)80001-8).
- [85] J.O. Valderrama, The state of the cubic equations of state, *Ind. Eng. Chem. Res.* 42 (2003) 1603–1618, doi: [10.1021/ie020447b](https://doi.org/10.1021/ie020447b).
- [86] J.O. Valderrama, A generalized Patel-Teja equation of state for polar and nonpolar fluids and their mixtures, *J. Chem. Eng. Jpn.* (1990), doi: [10.1252/jcej.23.87](https://doi.org/10.1252/jcej.23.87).
- [87] D.L. Wang, Vapor-liquid equilibrium studies on the system argon-oxygen, in: T.K.D. (Ed.), *Advances in Cryogenic Engineering*, Plenum Press, Inc., New York, 1960, pp. 294–295.
- [88] S. Wang, H. Xiang, B. Han, The modification and generalization of BWR equation, *Fluid Phase Equilib.* 181 (2001) 71–82, doi: [10.1016/S0378-3812\(01\)00359-4](https://doi.org/10.1016/S0378-3812(01)00359-4).
- [89] L.T. Watson, M. Bartholomew-Biggs, Nonlinear equations and optimisation, *J. Comput. Appl. Math.* 4 (2000) Elsevier Science B.V.

- [90] Ø. Wilhelmsen, A. Aasen, G. Skaugen, P. Aursand, A. Austegard, E. Aursand, M.A. Gjennestad, H. Lund, G. Linga, M. Hammer, Thermodynamic modeling with equations of state: present challenges with established methods, *Ind. Eng. Chem. Res.* 56 (2017) 3503–3515, doi: [10.1021/acs.iecr.7b00317](https://doi.org/10.1021/acs.iecr.7b00317).
- [91] D.S.H. Wong, S.I. Sandler, A theoretically correct mixing rule for cubic equations of state, *AIChE J.* 38 (1992) 671–680, doi: [10.1002/aic.690380505](https://doi.org/10.1002/aic.690380505).
- [92] H. Ye, J. Zheng, Y. Li, Feasibility analysis and simulation of argon recovery in low oxygen-purity cryogenic air separation process with low energy consumption, *Cryogenics* 97 (2019) 109–121, doi: [10.1016/j.cryogenics.2018.11.006](https://doi.org/10.1016/j.cryogenics.2018.11.006).
- [93] G. Zarca, I. Ortiz, A. Urtiaga, F. Llorell, Accurate thermodynamic modeling of ionic liquid/metal salt mixtures: application to carbon monoxide reactive absorption, *AIChE J.* 63 (2017) 3532–3543, doi: [10.1002/aic](https://doi.org/10.1002/aic).
- [94] X.Bin Zhang, J.Y. Chen, L. Yao, Y.H. Huang, X.J. Zhang, L.M. Qiu, Research and development of large-scale cryogenic air separation in china, *J. Zhejiang Univ. 15* (2014) 309–322, doi: [10.1631/jzus.A1400063](https://doi.org/10.1631/jzus.A1400063).
- [95] Y. Zhu, C. Laird, Optimal planning and operation of cryogenic air separation columns considering uncertain demands and product transitions, *AIChE Annual Meeting, Conference Proceedings*, 2008, p. 73601.
- [96] Y. Zhu, S. Legg, C.D. Laird, Optimal operation of cryogenic air separation systems with demand uncertainty and contractual obligations, *Chem. Eng. Sci.* 66 (2011) 953–963, doi: [10.1016/j.ces.2010.11.039](https://doi.org/10.1016/j.ces.2010.11.039).
- [97] Y. Zhu, S. Legg, C.D. Laird, Optimal design of cryogenic air separation columns under uncertainty, *Comput. Chem. Eng.* 34 (2010) 1377–1384, doi: [10.1016/j.compchemeng.2010.02.007](https://doi.org/10.1016/j.compchemeng.2010.02.007).